

Forschungszentrum Karlsruhe
Technik und Umwelt

Wissenschaftliche Berichte
FZKA 6256

**ITER ECRF Coaxial
Gyrotron and Window
Development (EU-T360)**

**Part I:
Coaxial Gyrotron Development**
– Final Report –

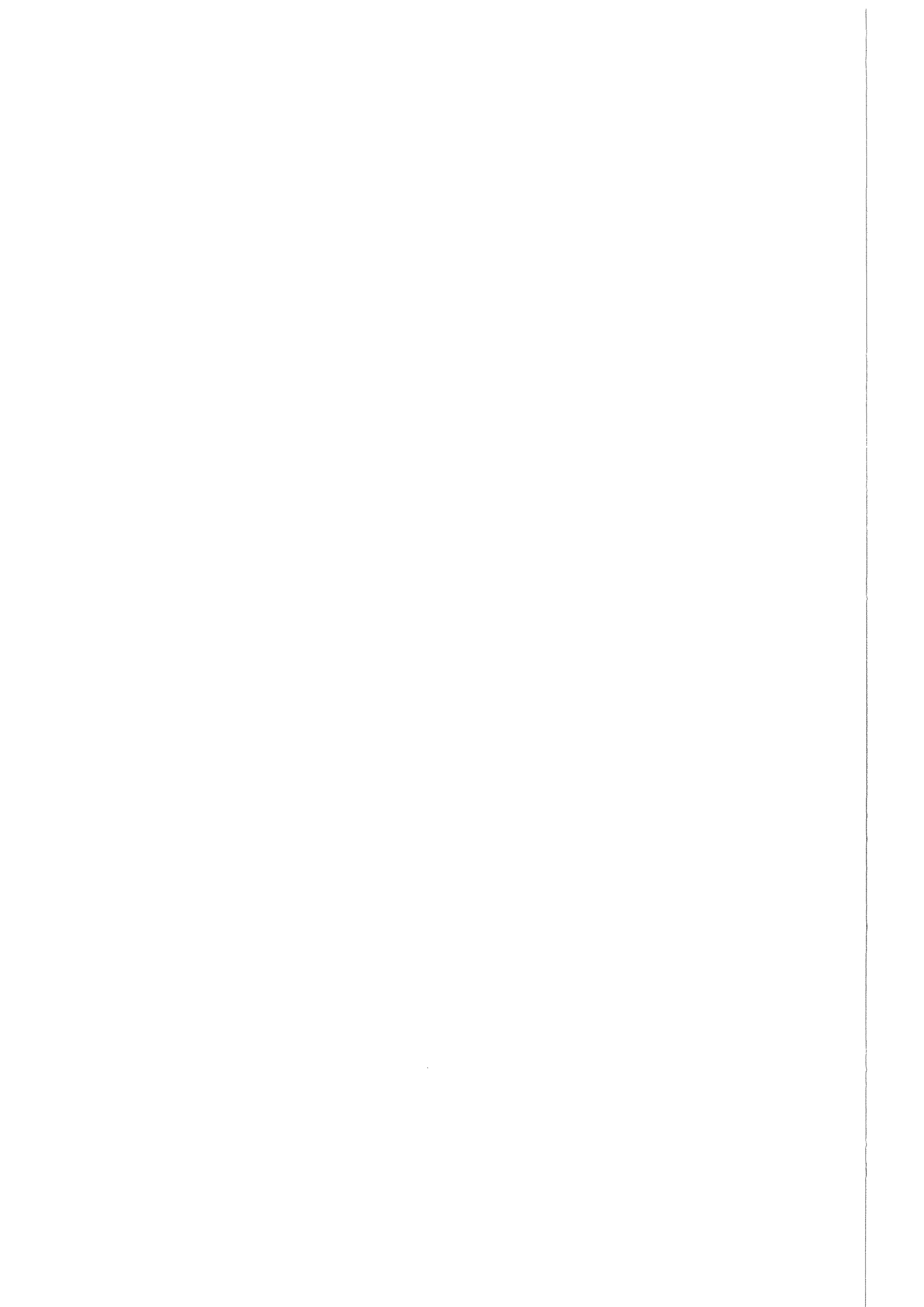
**B. Piosczyk, O. Braz, G. Dammertz,
M. Kuntze, G. Michel, A. Möbius, M. Thumm**

Institut für Technische Physik

Projekt Kernfusion

Association EURATOM-FZK

Februar 1999



Forschungszentrum Karlsruhe
Technik und Umwelt
Wissenschaftliche Bericht
FZKA 6256

**ITER ECRF COAXIAL GYROTRON AND WINDOW
DEVELOPMENT (EU-T360)**

Part I: Coaxial Gyrotron Development

- Final Report -

B. Piosczyk, O. Braz^{*}, G. Dammertz, M. Kuntze, G. Michel, A. Möbius, M. Thumm^{*}

Institut für Technische Physik

Projekt Kernfusion
Association EURATOM-FZK

^{*}also Universität Karlsruhe, Institut für Höchstfrequenztechnik und Elektronik

Forschungszentrum Karlsruhe GmbH, Karlsruhe
1999

Als Manuskript gedruckt
Für diesen Bericht behalten wir uns alle Rechte vor
Forschungszentrum Karlsruhe GmbH
Postfach 3640, 76021 Karlsruhe
Mitglied der Hermann von Helmholtz-Gemeinschaft
Deutscher Forschungszentren (HGF)
ISSN 0947-8620

ITER ECRF COAXIAL GYROTRON AND WINDOW DEVELOPMENT

Part I: Coaxial Gyrotron Development

- Final Report -

Task No.: G52 TT 14 FE

ID-No.: GB7 - EU - T360

Executive Summary:

Based on the experience gained with the inverse magnetron injection gun (IMIG) for coaxial cavity gyrotrons, a new 4.5 MW electron gun for operation at a cathode voltage of 90 kV and a beam current of 50 A has been designed and is currently under fabrication at Thomson Tubes Electroniques (TTE). The gun is of the diode type. Different from the LaB₆ IMIG currently used, the emission of the electrons will not be directed towards the coaxial insert but towards the anode similar like in conventional MIG gyrotron electron guns. The inner conductor is supported from the gun inner conductor side and can be aligned in a reproducible way in the fully assembled tube. The insert is cooled as required for operation at long pulses up to cw. The cathode will be equipped with an impregnated tungsten matrix emitter as used in industrial tubes.

A 160/170 GHz, 1.5 MW, 100 ms pulse length coaxial gyrotron employing the new electron gun and a single-stage depressed collector has been designed. The advanced quasi-optical converter for transforming the TE_{-31,17} cavity mode at 165 GHz into a single rf-output wave beam (only one output window) consists of a simple launcher and two mirrors. The first mirror is quasi-elliptical and the second mirror has a non-quadratic phase-correcting surface to generate an approximately homogeneous rf-field distribution with a high fundamental Gaussian content in the window plane.

First test experiments with the new gyrotron have been performed employing the available LaB₆-IMIG.

Following experimental results have been achieved:

RF-output power: $P_{\text{out}} = 1.2 \text{ MW}$

Output efficiency: $\eta = 25 \%$ without depressed collector,
 $\eta = 35 \%$ with single-stage depressed collector

For comparison of the experimental values with simulation calculations a selfconsistent, time dependent multimode code has been used with the experimental parameters taken as input. The measured value of the output power agrees well with the calculations at lower beam voltages. For the maximum output power the calculated values are about 15 % higher than in the experiment. An explanation for the discrepancy needs further investigations. Up to the applied retarding voltage at the collector of $U_{\text{coll}} \approx 31 \text{ kV}$ no decrease of the rf-power was

observed. In general, the measurements have been performed with pulses of 0.5 ms at 5 Hz. In single-pulse operation the pulse length was extended up to about 15 ms. Single-mode operation over a wide range ($\Delta U_c \cong 8$ kV) was observed. The measured rf-power distribution behind the window plane is in good agreement with numerical calculations. The overall rf-losses inside the tube (ohmic losses, absorption in the window and stray radiation due to diffraction losses) are calculated to about 12 % and have been included in the comparison of experiment and theory.

KOAXIALGYROTRON- UND FENSTER-ENTWICKLUNG FÜR ITER ECRF

Teil I: Koaxial-Gyrotron-Entwicklung

- Schlußbericht -

Task No.: G 52 TT 14 FE

ID-No.: GB6 – EU – T360

Kurzfassung:

Basierend auf der mit der "Inverse Magnetron Injection Gun" (IMIG) für Gyrotrons mit koaxialem Resonator gewonnenen Erfahrungen wurde eine neue 4,5 MW Elektronenkanone für den Betrieb bei einer Kathodenspannung von 90 kV und einem Strahlstrom von 50 A ausgelegt, die gegenwärtig bei Thomson Tubes Electroniques (TTE) hergestellt wird. Die Kanone ist vom Diodentyp. Anders als bei der derzeit verwendeten LaB₆ IMIG geschieht die Emission der Elektronen nicht in Richtung des koaxialen Einsatzes sondern gegen die Anode, ähnlich wie in konventionellen MIG-Elektronenkanonen für Gyrotrons. Der zentrale Innenleiter wird von der Kanonenseite her getragen und kann auf reproduzierbare Art und Weise, bei vollständig zusammengebauter Röhre, ausgerichtet werden. Der Einsatz wird so gekühlt, wie es für Langpuls- bzw. CW-Betrieb erforderlich ist. Die Kathode ist wie bei industriellen Röhren mit einem imprägnierten Wolfram-Matrix-Emitter ausgerüstet.

Es wurde ein Langpuls-160/170 GHz-1,5 MW Koaxialgyrotron für 100 ms Pulslänge ausgelegt, das mit der neuen Elektronenkanone und einem einstufigen Kollektor mit Gegenspannung ausgestattet ist. Der fortschrittliche quasi-optische Modenwandler, der die TE_{31,17}-Resonatormode bei 165 GHz in einen HF-Ausgangsstrahl (nur ein Ausgangsfenster) transformiert, besteht aus einem einfachen Launcher und zwei Spiegeln. Der erste Spiegel ist quasi-elliptisch und der zweite hat eine nicht-quadratische, phasenkorrigierende Oberfläche, um eine näherungsweise homogene HF-Feldverteilung mit hohem fundamentalen Gaußanteil an der Fensterebene zu erzeugen.

Erste Testexperimente mit dem neuen Gyrotron sind mit der bereits verfügbaren LaB₆-IMIG durchgeführt worden.

Dabei wurden folgende experimentellen Ergebnisse erzielt:

HF-Ausgangsleistung: $P_{\text{out}} = 1,2 \text{ MW}$

Ausgangswirkungsgrad: $\eta = 25 \%$ mit Kollektor ohne Gegenspannung

$\eta = 35 \%$ mit einstufigem Kollektor mit Gegenspannung

Zum Vergleich der experimentellen Ergebnisse mit Simulationsrechnungen wurde ein selbstkonsistentes, zeitabhängiges Multimoden-Programm benutzt, in dem die experimentellen Parameter als Eingangsgrößen verwendet wurden. Die gemessenen Werte der Ausgangsleistung stimmen bei niedrigen Beschleunigungsspannungen gut mit den Rechnungen überein. Bei der maximalen Ausgangsleistung sind die berechneten Werte ungefähr 15 % höher als im Experiment. Zur Erklärung dieser Diskrepanz sind weitere Untersuchungen erforderlich. Bis zu einer Kollektorgegenspannung von $U_{\text{coll}} \approx 31 \text{ kV}$ wird keine Abnahme der Ausgangsleistung beobachtet. Die Messungen wurden im allgemeinen mit Pulslängen von

0,5 ms bei 5 Hz durchgeführt. Im Einzelpulsbetrieb konnte die Pulslänge auf ungefähr 15 ns verlängert werden. Es wurde über einen sehr breiten Bereich ($\Delta U_c \cong 8 \text{ kV}$) Einmodenbetrieb beobachtet. Die hinter der Fensterebene gemessene HF-Leistungsverteilung ist in guter Übereinstimmung mit numerischen Berechnungen. Die gesamten HF-Verluste in der Röhre (ohmsche Verluste, Absorption im Fenster und Streustrahlung aufgrund von Beugungsverlusten) wurden zu ungefähr 12 % berechnet und beim Vergleich von Experiment und Theorie berücksichtigt.

Contents

Executive Summary

Kurzfassung

Report 1-2

Acknowledgments 3

Appendix A1

A 4.5 MW – electron gun for a coaxial gyrotron – results of design calculations 5-26

Appendix A2

A 4.5 MW – Electron Gun for a Coaxial Cavity Gyrotron 27-28

Appendix A3

165 GHz, $TE_{31,17}$ – Coaxial Cavity Gyrotron with Quasi-optical RF-Output 29-30

Appendix A4

Design of a Quasi-Optical Mode Converter for a Coaxial 165 GHz
 $TE_{31,17}$ Gyrotron 31-32

Appendix A5

Photograph of the quasi-optical $TE_{31,17}$ -to-wave beam converter 33

Appendix A6

Comparison of measured and calculated rf-power distribution in the window
plane 34

Report

Subtask 1: Design of improved electron gun for coaxial gyrotrons

In order to investigate the specific problems of a coaxial gyrotron, in particular in view of cw operation and to demonstrate a technically feasible solution a new 4.5 MW (90 kV, 50 A) electron gun has been designed and is now under fabrication at TTE. In particular the design of the cooling and of the possibility of reproducible adjustment of the coaxial insert and the cathode technology fulfil the requirements of cw-operation. Since the gun is foreseen to be used in an experimental set up at FZK the design of the gun is adapted to the existing equipment, in particular to the superconducting (sc) magnet.

The electron gun has two electrodes (diode type). The arrangement of the electron emitter ring and the anode is similar to that of a conventional magnetron injection gun (MIG) for gyrotrons. Thus, the emission of the electrons is not, as in the presently used inverse magnetron injection gun (IMIG) directed towards the inner rod but towards the anode. The suggested gun has the following important advantages over the IMIG gun geometry:

- reduced diameter of the gun at a given diameter of the emitter
- negligible influence of the inner rod on the beam properties
- possibility of independent polarization of the inner rod

The cathode will be equipped with an impregnated tungsten matrix emitter as used in industrial long pulse gyrotrons. Detailed informations about the design of the new gun are given in the appendices A1 and A2.

Subtask 2: Fabrication of a 1.5 MW, 165 GHz, 100 ms coaxial gyrotron

First experimental steps towards an operation of the coaxial gyrotron with pulses up to about 100 ms has been performed with the $TE_{-31,17}$ mode coaxial gyrotron at 165 GHz. The gyrotron has been equipped with the LaB_6 -IMIG and a q.o. system for transmission of the rf-power through a single window. The high volume cavity mode is directly transformed to a homogeneously distributed paraxial beam. The q.o. system consists of a Vlasov launcher with a single cut and two mirrors. The rf-power is radiated with a transverse angle of divergence of about 142° towards the first quasi-elliptic mirror. The second mirror has a phase-correcting surface in order to generate approximately a homogeneous rf-field distribution with a high Gaussian content in the window plane. Since the transmission for neighbouring cavity modes is good, frequency step tuning can be performed. Stray radiation due to diffraction losses has been estimated to $\leq 5\%$ and the absorption losses to about 7% resulting in total losses of about 12%. A fused silica window with a thickness of about 13 half wavelengths at 165 GHz is used.

The $TE_{31,17}$ mode has been found to oscillate with a frequency of 165.0 GHz in very good agreement with the design. A wide single mode operating range has been observed ($\Delta U_c \cong 8$ kV). A maximum rf-output power of 1.2 MW with an efficiency of 25% was measured. The single-stage depressed collector was used successfully, increasing the rf-output efficiency from 25 % to 35 %. In single pulses the pulse length has been extended up to about 15 ms limited by the capability of the HV power supply. Time consuming HV conditioning of the tube was necessary. For a further extension of the pulse length a modification of the HV

power supply is foreseen. The measured rf-power distribution in the window plane is in good agreement with numerical calculations. In order to improve the power distribution at the window a new phase corrected mirror has been designed and is under fabrication. For the design an improved code taking fully into account the wave optics has been used. More detailed results of the performed experiments are given in appendices A3, A4, A5 and A6.

Appendices:

- A1:** A 4.5 MW – electron gun for a coaxial gyrotron – results of design calculations-
- A2:** A 4.5 MW – Electron Gun for a Coaxial Cavity Gyrotron
- A3:** 165 GHz, $TE_{31,17}$ – Coaxial Cavity Gyrotron with Quasi-optical RF-Output
- A4:** Design of a Quasi-Optical Mode Converter for a Coaxial 165 GHz $TE_{31,17}$ Gyrotron
- A5:** Photograph of the quasi-optical $TE_{31,17}$ -to-wave beam converter
- A6:** Comparison of measured and calculated rf-power distribution in the window plane

Acknowledgments

This report is an account of work assigned as an ITER TASK to the European Home Team under the Agreement among the European Atomic Energy Community, the Government of Japan, the Government of the Russian Federation and the Government of the United States of America on Cooperation in the Engineering Design Activities for the International Thermonuclear Experimental Reactor ("ITER EDA Agreement") under the auspices of the International Thermonuclear Energy Agency (IAEA). The work was supported by the European Fusion Technology Program under the Projekt Kernfusion of the Forschungszentrum Karlsruhe. We gratefully acknowledge stimulating and useful discussions with colleagues from IAP, Nizhny Novgorod, in particular Drs. V. Flyagin, V. Khishnyak, A. Pavelyev and V. Zapevalov. The contributions of H. Baumgärtner, H. Budig, P. Grundel, H. Kunkel, W. Leonhardt, J. Szczesny and R. Vincon of the gyrotron team technical staff for the mechanical design, the precise machining and the careful assembly of the coaxial gyrotron as well as for their assistance during the experiments were essential for the success of the work. The authors thank Prof. E. Borie for proofreading of the manuscript.



A 4.5 MW - electron gun for a coaxial cavity gyrotron - results of design calculations -

B. Piosczyk

FZK-Karlsruhe, ITP, e-mail: piosczyk@itp.fzk.de

1. Introduction

The electron gun is of diode type. The arrangement of the emitter and the anode is similar as in a conventional (MIG) gun. The diameter of the cathode is sufficiently large in order to place the inner rod inside the cathode. Thus, the emission of the electrons is not directed as in the inverse magnetron injection gun (IMIG) towards the inner rod but towards the anode as in a conventional MIG gun. In operation the inner rod which is surrounded by the cathode is close to ground potential, in general. However, a positive polarization of the inner rod relative to the anode extends the variability of the operating conditions with interesting new features.

The design has been performed in order to satisfy the requirements on the electron beam as well for the $TE_{28,16}$ mode at 140 GHz and for the $TE_{31,17}$ mode at 165 GHz. This can be fulfilled by an individual optimization of the anode shape for the both cases but with unchanged surface contours of the cathode and the inner rod.

The arrangement of the emitter with the cathode and the anode similar as in a conventional MIG gun has the following advantages over the inverse gun arrangement:

- reduced diameter of the gun at a given diameter of the emitter
- much less influence of the inner rod on the beam properties
- possibility of independent polarization of the inner rod

The advantages are considered to be important. In particular the possibility of independent polarization of the inner rod opens new interesting properties of the gun as is discussed in a separate section at the end of this report.

Tab. 1: Geometry of the coils of the sc-magnet (cold geometry)

coil	$z_{\text{center}} / \text{cm}$	$r_{\text{center}} / \text{cm}$	$\Delta z / \text{cm}$	$\Delta r / \text{cm}$	n
main coil	37.922	19.595	30.058	4.297	17257
HS	37.922	22.917	30.058	2.347	9333
cancellation coil	14.149	20.259	8.033	5.625	6139
KS	12.213	23.112	4.161	0.082	46
upper gun coil GS2	4.976	24.066	1.791	1.137	1065
lower gun coil GS1	-0.796	24.216	4.578	1.438	1139

The design of the gun has been performed for a magnetic field distribution of an existing superconducting (sc) magnet. The magnet consist of three independent adjustable solenoidal coils. A main coil (HS) operated in series with a cancellation coil (KS) determines mainly the magnetic field around and above the cavity. The main and the cancellation coil are made internally out of two parts, each. With the two gun coils (GS1 and GS2) which are energized independently different field distributions in the gun region can be generated. The geometry of the coils is given in Tab. 1. z_{center} and r_{center} are the coordinate of the center of each solenoid, Δz and Δr are the axial and radial width of the coil and n is the number of turns. In the used

coordinate system the maximum of the magnetic field is close to $z_{\max} = 396$ mm. The center of the emitter has been placed at $z_e = 32$ mm. The warm bore hole of the sc-magnet has a diameter of 275 mm.

The gun design has been performed observing the following technical restrictions:

- radial extension of the gun as small as possible
- emitter current density $j_e \leq 3.5$ A/cm²
- maximum voltage at the surface of the electrodes $E_{\max} < 7$ kV/mm

2. Requirements on the electron beam

The generated electron beam has to be suitable for operation in the TE_{31,17} mode at 165 GHz and in the TE_{28,16} mode at 140 GHz. The required parameters are summarized in Tab.2. The nominal operating voltage has been chosen to be 90 kV. But since the maximum magnetic field achievable with the existing sc-magnet is only about 6.6 T, the optimization of the gun for operation at 165 GHz has been done for a voltage $U_c = 80$ kV corresponding to a required value of the magnetic field in the cavity of about $B_{\text{cav}} \cong 6.58$ T. The needed beam radius R_b in the cavity is different in both cases. Since the cathode radius stays unchanged a different magnetic compression has to be used. The radial extension of the electron beam is approximately $\lambda_0/8$ with λ_0 the free space wavelength.

Tab. 2: Required electron beam parameters

accelerating voltage :	U_c	=	90	kV
beam current :	I_b	=	50	A
desired velocity ratio :	α	\cong	1.4	
operating mode :			TE_{28,16}	TE_{31,17}
frequency :	f / GHz		140	165
magnetic field in the cavity :	B_{cav} / T		5.55	6.67
for $U_c = 80$ kV :	B_{cav} / T		-	6.58
average beam radius at the cavity :	R_b / mm		10.0	9.41
beam thickness (guiding centers) at cavity :	ΔR_b / mm		$\cong 0.23$	$\cong 0.23$

The magnetic field inside the cavity region is mainly determined by the current I(HS) in the main coil which is operated in series with the cancellation coil KS. Different magnetic field distributions can be adjusted in the gun region by using different currents I(GS1) and I(GS2) in the two gun coils. In Tab. 3 the currents in the coils and the corresponding magnetic field and magnetic compression ratio are given for field distributions b1(..) and b2(..) in which only one gun coil is energized. The magnetic compression is given by the square of the ratio of the emitter radius to the beam radius in the cavity, $b = \{R_e/R_b\}^2$. The distributions b2(140) and b2(165) are taken as reference distributions for the nominal calculations. An intermediate field

Tab. 3: The coil currents, the magnetic field and the magnetic compression ratio of investigated field distributions. The bold printed and shadowed lines represent the reference distributions.

mode		I(GS1) / A	I(GS2) / A	I(HS) / A	B_{cav} / T	$b = (R_e / R_b)^2$
TE _{28,16}	b1(140)	69.0	0.0	91.3	5.543	32.8
	b2(140)	0.0	71.0	91.3	5.552	32.6
TE _{31,17}	b1(165)	74.0	0.0	108.4	6.578	36.9
	b2(165)	0.0	75.8	108.4	6.587	36.9

distribution using both gun coils allows to influence the beam parameters within a certain range. If the currents in the gun coils are chosen according to equ. 1 then the beam radius in the cavity stays unchanged.

$$\begin{aligned}
 I(\text{GS1}) &= (1-x) \cdot 69.0 \text{ A} ; & I(\text{GS2}) &= x \cdot 71.0 \text{ A} & \text{for the TE}_{28,16} \text{ mode} \\
 I(\text{GS1}) &= (1-x) \cdot 74.0 \text{ A} ; & I(\text{GS2}) &= x \cdot 75.8 \text{ A} & \text{for the TE}_{31,17} \text{ mode} \\
 & & & & \text{with } 0 \leq x \leq 1
 \end{aligned} \tag{1}$$

3. Design of the gun

Two different guns are needed for generating the two different electron beams. As already mentioned, in the present design, the requirements for the two different electron beams can be fulfilled by using the same cathode and same inner rod for both cases. The individual adjustment for the operation in the two different modes is performed by replacement of the anode electrode with individually optimized surface contour. The Figs. 1a,b show the contours of the electrodes for the $\text{TE}_{28,16}$ mode and the $\text{TE}_{31,17}$ mode. The most interesting parameters of the designed gun are summarized in Tab.3. The Fig. 2 gives a schematic view of a possible layout of the gun.

Tab. 4: Design parameters of the IMIG-gun

cathode with emitter:

average radius of the emitter	R_c	=	57.2	mm
radial width	ΔR_c	=	1.6	mm
axial width	Δz_c	=	4.0	mm
emitting surface	F_c	=	15.5	cm ²
tilt angle ($\arctan \Phi_c = 0.4$)	Φ_c	=	21.80°	
diameter of the bore hole inside the cathode	D_c	=	79.2	mm

axial position:

axial position of the emitter center	z_c	=	32	mm
axial position of the maximum magnetic field	z_{max}	=	396	mm
distance between center of emitter and cavity	Δz_{ccav}	=	364	mm

4. Beam and gun parameters under nominal operating conditions

The electron gun has been optimized using the EGUN-code. The electron trajectories have been calculated from the gun up to the resonator. The calculations have been performed with a mesh size of 0.4 mm. The electron beam has been represented by 20 beamlets.

The electron trajectories together with the contours of the electrodes are shown in the Figs. 3 , 4 calculated for the nominal parameters. The electron trajectories are of non-laminar type as is demonstrated especially by the enlarged part of the trajectories in the mentioned figures. The nominal beam and operating gun parameters are summarized in Tab. 5. The values β_{\perp} and β_{\parallel} are averaged over the corresponding values of the single beamlets with $\alpha = \beta_{\perp}/\beta_{\parallel}$. The velocity spread $\delta\beta_{\perp\text{max}}$ is defined as: $\delta\beta_{\perp\text{max}} = (\beta_{\perp\text{max}} - \beta_{\perp}) / \beta_{\perp}$ and $\delta\beta_{\perp\text{rms}}$ is the rms-value calculated from the values of the single beamlets. $\beta_{\perp\text{max}}$ is related to the maximum α -value achievable without reflections, $\alpha_{\text{max}} = 1 / \{2\delta\beta_{\perp\text{max}}/\beta_{\perp}\}$. The maximum electric field is at the cathode nose and is approximately as at the inner rod. The field values for the $\text{TE}_{31,17}$ mode are slightly lower than for the $\text{TE}_{28,16}$ mode mainly due to the lower cathode voltage of 80 kV. The electric field E_c at the center of the emitter is calculated for a beam current of 50 A. It increases for zero current by about 10 %. For the nominal magnetic field distribution

the magnetic field lines at the emitter surface are directed towards the axis under about 3° . The direction varies over the emitter surface by about $\pm 1^\circ$.

The distribution of the transverse velocity versus the starting position at the emitter surface is shown in the Figs. 5a, b. The calculations have been performed with EGUN and for comparison also with the EPOSR-code and the BFCRAY-code*. The numerical results achieved with the three different codes are in reasonably good agreement.

Tab. 5: Nominal beam parameters and magnetic and electric fields inside the gun.
In brackets are the results of EPOSR and BFCRAY, respectively.

operating mode		TE _{28,16}	TE _{31,17}
beam parameters:			
beam current	I_b / A	50	50
current density	$j_c / A/cm^2$	3.2	3.2
cathode voltage	U_c / kV	90	80
magnetic field in the cavity	B_{cav} / T	5.55	6.58
transverse velocity	β_\perp	0.436	0.412
axial velocity	β_\parallel	0.284	0.284
velocity ratio	$\alpha = \beta_\perp / \beta_\parallel$	1.53 [1.38/ 1.35]	1.45 [1.38 / 1.33]
velocity spread - rms value	$\delta\beta_{\perp rms} / \%$	2.2 [0.7 / 2.0]	1.9 [2.0 / 1.6]
- max. value	$\delta\beta_{\perp max} / \%$	3.4 [1.3 / 3.0]	2.5 [3.8 / 4.4]
magnetic and electric fields inside the gun:			
axial magnetic field at z_e	B_c / T	0.187	
axial magnetic field at z_{max}	B_{cav} / T	5.55	6.58
maximum electric field			
at cathode surface	$E_{max} / kV/mm$	6.3	5.8
at emitter surface	$E_e / kV/mm$	3.6	3.5
at inner rod	$E_{rod} / kV/mm$	6.2	5.4
direction of the magnetic field :			
at the emitter center	$\varphi_B / ^\circ$	-3.1	-3.3
variation over the emitter	$\Delta\varphi_B / ^\circ$	-2.3 \rightarrow -4.0	-2.3 \rightarrow -4.3

5. Dependence of the electron beam on operating parameters

A small sensitivity of the beam parameters with respect to variation of operating parameters is of great importance for the usability of a gun. Therefore, numerous calculations have been done to investigate the influence of a variation of the operating parameters on the beam properties. The results are given in this section.

According to adiabatic theory of electron motion the transverse velocity β_\perp of the diode gun should depend on the operating parameters as:

$$\beta_\perp \propto \frac{1}{\gamma_0} \frac{B_{cav}^{1/2}}{B_e^{3/2}} U_c \cos \varphi_{EB} \approx \frac{1}{\gamma_0} \frac{b^{1/2}}{B_e} U_c \cos \varphi_{EB} \quad (2)$$

$\varphi_{EB} = \Phi_c + \varphi_B$ is the angle between the electric and magnetic field at the emitter surface. The tilt angle of the emitter is $\Phi_c = 21.8^\circ$ and φ_B is the angle between the magnetic field and the emitter surface. The angle φ_{EB} varies between about 18.2° and 24.0° for the field distributions

* calculations with BFCRAY have been performed by Dr. E. Borie

b2(140), b2(165) and b1(140), b1(165), respectively. B_e is the magnetic field at the emitter and b the magnetic compression ratio. γ_0 is the relativistic mass factor.

5.1 Dependence on beam current I_b :

The calculations (Tab. 6) have been performed with the nominal parameters. Due to the influence of the space charge effect the values of α and β_{\perp} are decreasing with increasing beam current. Correspondingly the electric field decreases by about 10% for $I_b = 50$ A relative to zero current causing in reasonably good agreement with the adiabatic relation (equ.2), a decrease of β_{\perp} by about 7%. The velocity spread has its minimum around the nominal current. The results are also presented in Fig. 6. The value of $\beta_0 = 0.52$ and 0.49 for 90 kV and 80 kV, respectively, indicate the limit of β_{\perp} where reflections at the magnetic mirror occur.

Tab. 6: The beam parameters versus the beam current I_b . The bold printed and shadowed line corresponds to the reference value.

a) TE_{28,16} at 140 GHz for b2(140) and $U_c = 90$ kV :

I_b [A]	α	β_{\perp}	$\beta_{ }$	$\delta\beta_{\perp,rms}$ [%]	$\delta\beta_{\perp,max}$ [%]
<0.1	1.93	0.466	0.241	4.0	4.1
20	1.73	0.453	0.262	3.0	3.5
30	1.64	0.446	0.272	2.5	3.6
40	1.58	0.441	0.279	2.2	3.4
50	1.53	0.436	0.284	2.2	3.4
60	1.46	0.428	0.294	3.0	3.7

b) TE_{31,17} at 165 GHz for b2(165) and $U_c = 80$ kV :

I_b [A]	α	β_{\perp}	$\beta_{ }$	$\delta\beta_{\perp,rms}$ [%]	$\delta\beta_{\perp,max}$ [%]
<0.1	2.24	0.456	0.204	5.1	7.9
20	1.86	0.440	0.237	3.8	5.7
30	1.70	0.431	0.254	3.1	3.7
40	1.55	0.421	0.271	2.3	3.1
50	1.45	0.412	0.284	1.9	2.9
60	1.36	0.403	0.296	2.5	3.5

5.2 Dependence on cathode voltage U_c :

For these calculations the cathode voltage has been varied between 70 kV and 100 kV with $I_b = 50$ A. The results are given in Tab.7. The velocity ratio α increases with the beam voltage in qualitative agreement with the adiabatic approximation given in equ. 2. The calculations have been performed for the nominal position of the emitter ($z_e = 32$ mm) and for positions shifted by ± 2 mm. The velocity spreads $\delta\beta_{\perp,rms}$ and $\delta\beta_{\perp,max}$ have approximately their minimum value at the nominal parameters. The variation of the emitter position leads only to modest variations of the beam parameters. Therefore, an uncertainty of the emitter position of ± 2 mm can be accepted. At a cathode voltage $U_c \geq 95$ kV at the TE_{28,16} mode and $U_c \geq 85$ kV at the TE_{31,17}-mode it may become difficult to operate the gun because of the high α -value. If operation at the high cathode voltage were to be required the α -value may have to be reduced by using a different magnetic field distributions in the gun region as is discussed in the

following sections. If at the TE_{31,17} mode at U_c = 90 kV the magnetic field is raised to 6.673 T as needed for compensation of the higher γ -value then α is reduced from 2.98 to 2.35.

Tab. 7: The beam parameters versus the cathode voltage U_c. The bold printed and shadowed line corresponds to the reference value.

a) TE_{28,16} at 140 GHz for b2(140) and I_b = 50 A :

U _c [kV]	z _e [mm]	α	β_{\perp}	β_{\parallel}	$\delta\beta_{\perp rms}$ [%]	$\delta\beta_{\perp max}$ [%]
100	30	2.06	0.487	0.236	3.6	3.9
	32	2.26	0.495	0.219	3.6	3.6
	34	2.38	0.499	0.210	3.1	4.0
95	30	1.80	0.464	0.259	2.5	3.2
	32	1.83	0.466	0.255	2.8	3.6
	34	1.82	0.466	0.256	2.5	3.6
90	30	1.53	0.434	0.284	2.2	3.0
	32	1.53	0.436	0.284	2.2	3.4
	34	1.47	0.431	0.293	2.4	4.2
85	30	1.30	0.404	0.310	2.3	3.5
	32	1.27	0.400	0.315	1.9	3.5
	34	1.22	0.394	0.324	2.6	4.6
80	30	1.10	0.368	0.334	2.8	3.8
	32	1.05	0.361	0.343	2.1	3.6
	34	1.01	0.354	0.349	2.8	4.0
75	30	0.93	0.330	0.355	3.3	6.4
	32	0.89	0.323	0.362	2.3	4.0
	34	0.85	0.315	0.369	3.3	6.0

b) TE_{31,17} at 165 GHz for b2(165) and I_b = 50 A :

U _c [kV]	z _e [mm]	α	β_{\perp}	β_{\parallel}	$\delta\beta_{\perp rms}$ [%]	$\delta\beta_{\perp max}$ [%]
90	30	reflections				
	32	2.98	0.494	0.166	2.0	2.8
	34	2.51	0.486	0.194	1.2	2.7
85	30	reflections				
	32	1.93	0.454	0.236	1.9	2.9
	34	1.74	0.444	0.255	1.8	3.8
80	30	1.53	0.418	0.274	3.1	4.5
	32	1.45	0.412	0.284	1.9	2.9
	34	1.37	0.403	0.295	3.0	6.0
75	30	1.25	0.380	0.304	3.3	6.1
	32	1.17	0.370	0.317	1.8	2.7
	34	1.12	0.363	0.324	4.4	8.5
70	30	1.04	0.340	0.328	3.5	6.2
	32	0.99	0.333	0.335	3.3	5.7
	34	0.96	0.326	0.341	6.7	12.3

5.3 Dependence on value of the magnetic field

5.3.1 Influence of the amplitude of the magnetic field

The calculation have been performed with the nominal operating parameters with the field distribution b2(140) and b2(165), respectively. The absolute value of the magnetic field has been varied by the factor (B / B_{nom}) . The nominal field amplitude is given by $B / B_{nom} = 1$. The results are summarized in Tab. 8. With decreasing (increasing) amplitude of the magnetic field the beam parameters α and β_{\perp} are increasing (decreasing) as expected from equ. 2. However, the dependence is stronger (approximately $\sim [B/B_{nom}]^{-2}$) than $\sim [B/B_{nom}]^{-1}$ as expected according equ.2 for adiabatic behaviour.

Tab. 8: Dependence of the beam parameters on the value of the magnetic field. The bold printed and shadowed line corresponds to the reference value.

a) TE_{28,16} at 140 GHz for b2(140) with $U_c = 90$ kV and $I_b = 50$ A :

B / B_{nom}	α	β_{\perp}	$\beta_{ }$	$\delta\beta_{\perp,rms}$ [%]	$\delta\beta_{\perp,max}$ [%]
0.94	2.49	0.479	0.193	4.7	5.0
0.96	2.02	0.465	0.230	3.6	4.1
0.98	1.72	0.449	0.261	2.8	3.3
1.00	1.53	0.436	0.284	2.2	3.4
1.02	1.36	0.419	0.309	2.1	3.8
1.04	1.21	0.401	0.333	2.1	4.0
1.06	1.09	0.385	0.353	2.5	3.9

b) TE_{31,17} at 165 GHz for b2(165) with $U_c = 80$ kV and $I_b = 50$ A :

B / B_{nom}	α	β_{\perp}	$\beta_{ }$	$\delta\beta_{\perp,rms}$ [%]	$\delta\beta_{\perp,max}$ [%]
0.94	2.85	0.468	0.164	2.6	3.6
0.96	2.11	0.450	0.213	2.2	3.6
0.98	1.70	0.431	0.253	2.2	3.0
1.00	1.45	0.412	0.284	1.9	2.9
1.02	1.27	0.393	0.309	1.9	3.1
1.04	1.16	0.379	0.327	1.7	2.6
1.06	1.06	0.364	0.342	1.8	2.7

5.3.2 Influence of the magnetic field distribution in the gun region

By generation of a different magnetic field distribution in the gun region either by energizing only the lower gun coil, b1(140), or by a combination of the currents in the both gun coils according to equ. 1, the beam parameters can be influenced within a certain range even if the magnetic field B_{cav} and the beam radius R_b in the cavity are kept constant. The calculations have been performed for the nominal emitter position and positions shifted by ± 2 mm. The generation of the magnetic field in the gun region has been changed stepwise from the coil GS2 {b2(140); b2(165) $\equiv x=1$ } to GS1 {b1(140); b1(165) $\equiv x=0$ }. The velocity ratio decreases for $x \leq 0.75$. For the distribution b1(140) and b1(165) the velocity ratio is as low as $\alpha = 0.87$ and 1.08, respectively. Thus by using different currents in the gun coils an adjustment of the values of α and β_{\perp} independently of the other parameters (cathode voltage, magnetic compression, magnetic field in the cavity) becomes possible. The amount of reduction of α and β_{\perp} by changing x from 1 to 0 is much higher than one would expect for adiabatic behaviour (equ.2) from the variation of ϕ_{EB} and the value of the magnetic field at

x	I(GS2)/I(GS1) [A]	z _c [mm]	α	β _⊥	β	δβ _{Lrms} [%]	δβ _{Lma} x [%]
1	71.0 / 0	30	1.53	0.434	0.284	2.2	3.0
		32	1.53	0.436	0.284	2.2	3.4
		34	1.47	0.431	0.293	2.4	4.2
0.9	63.90 / 6.90	30	1.51	0.434	0.288	2.9	4.4
		32	1.58	0.440	0.279	2.3	3.0
		34	1.58	0.440	0.279	1.8	3.2
0.75	53.25 / 17.25	30	1.41	0.425	0.301	3.1	3.8
		32	1.50	0.433	0.289	2.9	4.6
		34	1.60	0.441	0.276	2.2	3.9
0.50	35.50 / 34.50	30	1.17	0.396	0.339	3.8	5.1
		32	1.32	0.416	0.314	3.6	4.3
		34	1.49	0.432	0.290	3.5	4.9
0.25	17.75 / 51.75	30	0.93	0.355	0.384	3.0	4.2
		32	1.07	0.381	0.357	3.5	5.8
		34	1.27	0.408	0.324	3.6	3.9
0.10	7.10 / 62.10	30	0.78	0.323	0.412	4.2	6.5
		32	0.95	0.360	0.379	3.2	4.7
		34	1.16	0.395	0.341	3.1	4.8
0	0.00 / 69.00	30	0.70	0.300	0.429	6.1	7.7
		32	0.87	0.344	0.394	5.0	7.6
		34	1.10	0.389	0.350	3.8	5.1

a) TE_{28,16} at 140 GHz with U_c = 90 kV and I_b = 50 A

x	I(GS2)/I(GS1) [A]	z _c [mm]	α	β _⊥	β	δβ _{Lrms} [%]	δβ _{Lma} x [%]
1	75.8 / 0	30	1.53	0.418	0.274	3.1	4.5
		32	1.45	0.412	0.284	1.9	2.9
		34	1.37	0.403	0.295	3.0	6.0
0.9	68.22 / 7.40	30	1.61	0.424	0.263	4.8	7.8
		32	1.59	0.423	0.266	3.2	5.4
		34	1.48	0.413	0.280	2.4	4.1
0.75	56.85 / 18.50	30	1.59	0.423	0.267	2.9	4.3
		32	1.63	0.426	0.261	2.9	4.9
		34	1.61	0.425	0.263	2.0	2.6
0.50	37.90 / 37.00	30	1.43	0.410	0.286	4.5	6.1
		32	1.54	0.419	0.272	3.8	4.1
		34	1.71	0.431	0.252	3.1	5.6
0.25	18.95 / 55.50	30	1.16	0.378	0.327	4.2	6.1
		32	1.33	0.399	0.300	4.5	8.5
		34	1.58	0.422	0.266	4.1	6.6
0.10	7.58 / 66.60	30	0.97	0.348	0.357	5.2	6.9
		32	1.19	0.382	0.322	4.5	7.3
		34	1.45	0.411	0.283	4.4	6.8
0	0.00 / 74.00	30	0.87	0.328	0.376	4.9	8.2
		32	1.08	0.366	0.339	5.3	8.5
		34	1.38	0.404	0.293	4.2	5.7
0*	0.00 / 74.00	30	1.06	0.382	0.358	4.6	7.3
		32	1.46	0.432	0.295	3.9	7.4
		34	2.26	0.477	0.211	2.9	4.4

b) TE_{31,17} at 165 GHz with U_c = 80/90 kV and I_b = 50 A :

Tab. 9: Influence of different energizing of the gun coils IGS(1) and IGS(2) according to equ. 1 on beam parameters. * U_c = 90 kV

the emitter surface. There seems to be a contribution related to the different kind of the electron flow for the two distributions. Fig.8 shows the electron trajectories near the cathode calculated for the field distributions b1(140) and b1(165). Due to the larger angle φ_{EB} the electron flow is approximately quasilaminar compared to the non laminar flow for the distributions b2(140) and b2(165) as shown in the Figs. 3, 4.

5.3.3 Variation of the beam radius R_b in the cavity

The calculations have been performed for magnetic field distributions achieved by current in only one gun coil, either GS1 or GS2. The current in the main coil and therefore the magnetic field B_{cav} has been kept constant. The results are given Tab.10. The behaviour is in qualitative

Tab. 10: Dependence of the beam parameters on the beam radius in the cavity with. The bold printed and shadowed line corresponds to the reference value.

a) $TE_{28,16}$ at 140 GHz with $U_c = 90$ kV and $I_b = 50$ A :

$I(GS2)$ [A]	R_b [mm]	α	β_{\perp}	β_{\parallel}	$\delta\beta_{\perp rms}$ [%]	$\delta\beta_{\perp max}$ [%]
69.0	9.85	2.11	0.470	0.223	3.3	4.0
70.0	9.93	1.78	0.453	0.255	2.9	3.8
71.0	10.02	1.53	0.436	0.284	2.2	3.4
72.0	10.10	1.37	0.421	0.308	2.5	4.5
73.0	10.18	1.17	0.398	0.340	2.5	4.0
I(GS1)						
65.0	9.65	2.05	0.468	0.228	3.0	5.1
66.0	9.74	1.42	0.427	0.301	3.2	4.9
67.0	9.82	1.14	0.393	0.345	5.0	5.6
69.0	9.99	0.87	0.344	0.394	5.0	7.6

b) $TE_{31,17}$ at 165 GHz with $U_c = 90$ kV and $I_b = 50$ A :

$I(GS2)$ [A]	R_b [mm]	U_c [kV]	α	β_{\perp}	β_{\parallel}	$\delta\beta_{\perp rms}$ [%]	$\delta\beta_{\perp max}$ [%]
73.3	9.22	75	1.78	0.421	0.237	3.3	6.9
73.3	9.22	80	reflections				
74.55	9.32		1.82	0.437	0.240	2.6	3.2
75.8	9.41		1.45	0.412	0.284	1.9	2.5
77.05	9.50		1.27	0.392	0.308	1.7	2.8
78.3	9.59		1.13	0.373	0.330	2.3	2.7
80.8	9.77		0.91	0.335	0.369	3.5	6.6
I(GS1)							
70	9.10	80	reflections				
71	9.18		1.78	0.433	0.243	3.8	5.5
72.5	9.30		1.30	0.395	0.304	3.9	5.8
74	9.41		1.08	0.366	0.339	5.3	8.5

agreement with the adiabatic motion. However, the change of the α -value is stronger than expected from equ.2 because of the different magnetic compression. With the field distribution b2(140) an operation up to about $R_b \cong 9.8$ mm is expected to be possible at U_c

= 90 kV. The operation can be extended towards $R_b \approx 9.7$ mm with the distribution b1(140). For $R_b \approx 10.2$ mm the velocity ratio decreases to $\alpha \approx 1$ for the TE_{28,16} mode. For the TE_{31,17}-mode α increases to about 1.8 at $R_b = 9.2$ mm.

5.3.4: Influence of the emitter position z_e relative to the magnetic field:

The axial position of the emitter relative to the axial position of the coils is uncertain mainly due to the inaccurate knowledge of the axial position of the coils. The axial frame of the coils is defined by the geometry as given in Tab.1. The position z_e of the emitter has been varied relative to the position of the sc-coils. As a reference value $z_e = 32$ mm is taken.

Tab. 11: Influence of an axial shift on the beam parameters.

a) TE_{28,16} at 140 GHz with $U_c = 90$ kV and $I_b = 50$ A

z_e [mm]	α	β_{\perp}	β_{\parallel}	$\delta\beta_{\perp,rms}$ [%]	$\delta\beta_{\perp,max}$ [%]
b2(140) $\equiv I(HS) / I(ES2) / I(ES1) = 91.3 / 71.0 / 0.0$ A					
24	1.47	0.431	0.292	3.4	3.9
28	1.51	0.434	0.287	2.8	4.4
30	1.53	0.434	0.284	2.2	3.0
32	1.53	0.436	0.284	2.2	3.4
34	1.47	0.431	0.293	2.4	4.2
36	1.36	0.421	0.308	3.1	4.3
b1(140) $\equiv I(HS) / I(ES2) / I(ES1) = 91.3 / 0.0 / 69.0$ A					
24	0.48	0.226	0.472	9.9	15.9
28	0.56	0.257	0.456	6.0	9.3
30	0.70	0.300	0.429	6.1	7.7
32	0.87	0.344	0.394	5.0	7.6
34	1.10	0.389	0.350	3.8	5.1
36	1.39	0.423	0.304	2.8	3.5

a) TE_{31,17} at 165 GHz with $U_c = 80$ kV and $I_b = 50$ A

z_e [mm]	α	β_{\perp}	β_{\parallel}	$\delta\beta_{\perp,rms}$ [%]	$\delta\beta_{\perp,max}$ [%]
b2(165) $\equiv I(HS) / I(ES2) / I(ES1) = 108.4 / 75.8 / 0.0$ A					
24	1.62	0.425	0.262	2.6	4.2
28	1.64	0.426	0.260	2.4	5.2
30	1.53	0.418	0.274	3.1	4.5
32	1.45	0.412	0.284	1.9	2.9
34	1.37	0.403	0.295	3.0	6.0
36	1.24	0.388	0.313	5.1	8.5
b1(165) $\equiv I(HS) / I(ES2) / I(ES1) = 108.4 / 0.0 / 74.0$ A					
28	0.73	0.295	0.403	4.8	9.2
30	0.87	0.328	0.376	4.9	8.2
32	1.08	0.366	0.339	5.3	8.5
34	1.38	0.404	0.293	4.2	5.6
36	1.81	0.436	0.241	3.7	4.8

The position of the cavity is assumed to coincide with the maximum of the magnetic field $z_{\max} \cong 396$ mm. The calculations have been performed with the nominal parameters for both field distributions b1(140), b1(165) and b2(140), b2(165), respectively. The results are summarized in Tab.11. The sensitivity of the beam parameters to an axial misalignment is fairly low allowing an uncertainty in displacement up to ± 2 mm. This value of uncertainty in the axial position has a negligibly small ($< \pm 0.02$ mm) influence on the beam radius R_b .

6. Operation of the coaxial gyrotron with a polarized inner rod

The existence of the inner rod is an additional mechanical complication of a coaxial gyrotron compared with a conventional one. However, the presence of the inner rod may offer some advantages in operation. In particular, in the suggested design of the gun a polarization of the inner rod with respect to the anode enables a variation of the electron beam energy with nearly no influence on the transverse momentum $p_{\perp} \sim \beta_{\perp}$. This is similar to the behaviour of a triode gun where the voltage between the cathode and the modulation anode mainly determines β_{\perp} and the beam energy is given by the voltage between the cathode and the anode. A polarization of the inner rod can be done with a nearly powerless supply because the current I_{rod} to the inner rod is small. A value of $I_{\text{rod}} \leq 0.1 \% I_b$ was observed in experiments.

In the case of the coaxial arrangement the energy eU_b of the electrons inside the cavity is determined by the difference between the potential U_c of the cathode and the potential $V(R_b)$ at the beam position. The radial potential distribution $V(r)$ inside the cavity is given to a very good approximation by assuming cylindrical symmetry for the cavity geometry. The outer cavity wall ($r = R_{\text{cav}}$) is grounded: $V(R_{\text{cav}}) = 0$. At the inner rod the potential is given by the applied voltage $V_{\text{rod}} = V_0$. The radial dependence inside the cavity is represented by:

$$V(r) = \{V_0 / \ln(R_{\text{rod}}/R_{\text{cav}})\} \cdot \ln(r/R_{\text{cav}}) \quad (4)$$

with R_{cav} and R_{rod} the radius of the cavity and the inner rod, respectively. The voltage depression due to beam space charge is not considered here. The energy of the beam is given by: $eU_b = e|U_c| + eV(R_b)$. Due to the radial extension of the electron beam an energy spread ΔV_b is introduced because of the radial variation of $V(r)$ according to:

$$\Delta V_b = \{V_0 / \ln(R_{\text{rod}}/R_{\text{cav}})\} \cdot (\Delta R_b/R_b) \quad (5)$$

The radial width ΔR_b of the electron beam inside the cavity is about ± 0.2 mm including the spread in guiding centers due to the finite width of the emitter and taking into account the electron Larmor radius. In practice the effective width is larger due to misalignment between the beam and the cavity. The main contribution comes from the misalignment of the inner rod, $\Delta R_{\text{beff}} = \Delta R_{\text{bmis}} + \Delta R_b$. For other reasons the value of misalignment must not exceed $\Delta R_{\text{bmis}} = \pm 0.5$ mm. From the experimental experience with the coaxial gyrotron it is thought that a value of radial misalignment ≤ 0.2 mm is technically feasible.

For illustration, calculations have been done with the gun design for the $TE_{31,17}$ mode. The cathode voltage has its nominal value of $U_c = 80$ kV. The polarization of the inner rod has been varied between $U_{\text{rod}} = +20$ kV and -10 kV. The results are summarized in Tab.12. The effect of voltage depression $\Delta V_{\text{sc}} \cong 1.5$ kV is included in the numerically calculated value of the beam energy $eU_{\text{bsc}} = e(|U_c| + V(R_b) + \Delta V_{\text{sc}})$. The energy spread ΔU_{bsc} is mainly determined by the space charge effect. The contribution from the radial variation of the

potential inside the cavity has been calculated to be $< \pm 0.2$ keV for $U_{rod} = 20$ kV. The accuracy of the numerical calculation is about ± 0.1 keV.

In Tab. 13 the analytically calculated values (equ. 4,5) of the energy eU_b and energy spread $e\Delta U_b$ are given for the same operating voltages as in Tab. 12. The values of energy eU_b in Tab. 13 are higher by about 1 keV than in Tab. 12 because the effect of voltage depression is not considered in equ. 4. The energy spread introduced by the radial dependence of the potential inside the cavity has been calculated for three different radial widths - the intrinsic beam width of ± 0.2 mm, an effective width of ± 0.45 mm and a maximum effective width of ± 0.7 mm. Even in the case of the maximum effective width the introduced energy spread is only 1.2 % at $U_{rod} = 20$ kV. Therefore, no limitation on the gyrotron operation is expected from the introduced additional energy spread.

Tab. 12: The beam parameters versus the voltage U_{rod} . The bold printed and shadowed line corresponds to the reference value. TE_{31,17} mode with b2(165), $U_c = 80$ kV and $I_b = 50$ A.

$U_c + U_{rod}$ [kV]	U_{rod} [kV]	U_{bsc} [keV]	$\pm \Delta U_{bsc}$ [keV]	α	β_{\perp}	β_{\parallel}	$\delta\beta_{\perp,rms}$ [%]	$\delta\beta_{\perp,max}$ [%]
100	20.0	95.1	0.45	1.23	0.418	0.339	2.3	3.3
95	15.0	90.9	0.4	1.28	0.416	0.327	2.1	3.1
90	10.0	86.9	0.35	1.31	0.413	0.315	2.0	3.6
85	5.0	82.5	0.45	1.39	0.414	0.298	2.1	3.6
80	0.0	78.5	0.5	1.45	0.412	0.284	1.9	2.9
75	-5.0	74.3	0.55	1.54	0.410	0.266	1.9	3.4
70	-10.0	70.2	0.6	1.63	0.407	0.249	1.9	2.7

Tab. 13: The energy and energy spread of the beam for different voltages U_{rod} performed for the TE_{31,17} at 165 GHz with $R_{cav} = 27.38$ mm, $R_{rod} = 7.32$ mm and $R_b = 9.41$ mm.

$U_c + U_{rod}$ [kV]	U_{rod} [kV]	eU_b [keV]	V_b [kV]	$\pm e\Delta U_b$ [keV]			$\pm \Delta U_b / U_b$ [%]		
				$\pm \Delta R_{beff}$ [mm]			$\pm \Delta R_{beff}$ [mm]		
				0.2	0.45	0.7	0.2	0.45	0.7
100	20.0	96.2	16.2	0.32	0.73	1.13	0.33	0.8	1.2
95	15.0	92.1	12.1	0.24	0.54	0.85	0.26	0.6	0.9
90	10.0	88.1	8.1	0.16	0.36	0.56	0.18	0.41	0.64
85	5.0	84.0	4.0	0.08	0.18	0.28	0.1	0.21	0.33
80	0.0	80.0	0	0.0	0.0	0.0	0.0	0.0	0.0
75	-5.0	76.0	-4.0	-0.08	-0.18	-0.28	0.11	0.24	0.37
70	-10.0	71.9	-8.1	-0.16	-0.36	-0.56	0.22	0.50	0.78

A further advantage of operation with a polarized inner rod is an enhancement of the efficiency as in a operation with a single stage depressed collector (SDC). The positive polarization of the rod results in an increase of the beam energy inside the cavity by $eV(R_b)$. This part of the beam energy is recovered in a similar manner as in a operation with a depressed collector before the electron beam is dissipated at the grounded walls of the collector. This means that the total efficiency is increased similarly to operation with a SDC but without the need for a collector insulated relative to the body. When using a collector with

one insulating gap, a further increase of the rf-output efficiency compared to a two-stage depressed collector can be realized in a relatively simple way.

7. Summary

An electron gun for a coaxial cavity gyrotron has been designed. The electron beam is emitted towards the anode as in a conventional MIG gun. The different requirements on the beam for operation in both the $TE_{28,16}$ mode at 140 GHz and in the $TE_{31,17}$ mode at 165 GHz can be fulfilled with the same geometry of the cathode with the emitter and of the inner rod by using only a different shape of the anode optimized individually for the two cases. The achieved beam parameters are acceptable for efficient gyrotron operation in both modes.

The advantages of the chosen arrangement in comparison to the inverse (IMIG) gun are:

- reduced diameter of the gun at a given diameter of the emitter
- nearly no influence of the inner rod on the beam properties
- possibility of independent polarization of the inner rod.

The operation with a positively polarized inner rod has been investigated numerically. It offers the possibility of an additional adjustment of the beam parameters. Operation with a positively polarized inner rod is similar to operation with a single-stage depressed collector with the collector at ground and the body at positive potential relative to the collector. It opens also the possibility of a further increase of the output efficiency by applying a two-stage recovery system in a technical relatively simple manner.

Figures:

Fig. 1a: Electron gun for the TE_{28,16} mode - layout of the inner contours of the electrodes

Fig. 1b: Electron gun for the TE_{31,17} mode - layout of the inner contours of the electrodes

Fig. 2: Schematic view of the gun

Fig. 3: TE_{28,16} mode gun - Electron trajectories at nominal conditions. 1MU = 0.4 mm.
(a) trajectories in the gun; (b) trajectories near the emitter -enlarged scale

Fig. 4: TE_{31,17} mode gun - Electron trajectories at nominal conditions. 1 MU = 0.4 mm.
(a) trajectories in the gun ; (b) trajectories near the emitter - enlarged scale

Fig. 5: The transverse velocity β_{\perp} versus the starting position at the emitter surface calculated for the nominal parameters. (a) : TE_{28,16} mode gun with $I_b = 50$ A, $U_c = 90$ kV and b2(140) ; (b) TE_{31,17}-mode with $I_b = 50$ A, $U_c = 80$ kV and b2(165)

Fig. 6: α , β_{\perp} and $\delta\beta_{\perp,rms}$ versus I_b . β_0 corresponds to the electron energy eU_c . (a) TE_{28,16} mode gun with $U_c = 90$ kV and b2(140) ; (b) TE_{31,17} mode gun with $U_c = 80$ kV and b2(165)

Fig. 7: α , β_{\perp} and $\delta\beta_{\perp,rms}$ versus U_c . β_0 corresponds to the electron energy eU_c . (a) TE_{28,16} mode gun with $I_b = 50$ A and b2(140); (b) TE_{31,17} mode gun with $I_b = 50$ A and b2(165)

Fig. 8: Electron trajectories near the emitter for the b1(...) distributions. 1MU = 0.4 mm.
a) TE_{28,16} mode gun with b1(140); b) TE_{31,17} mode gun with b1(165)

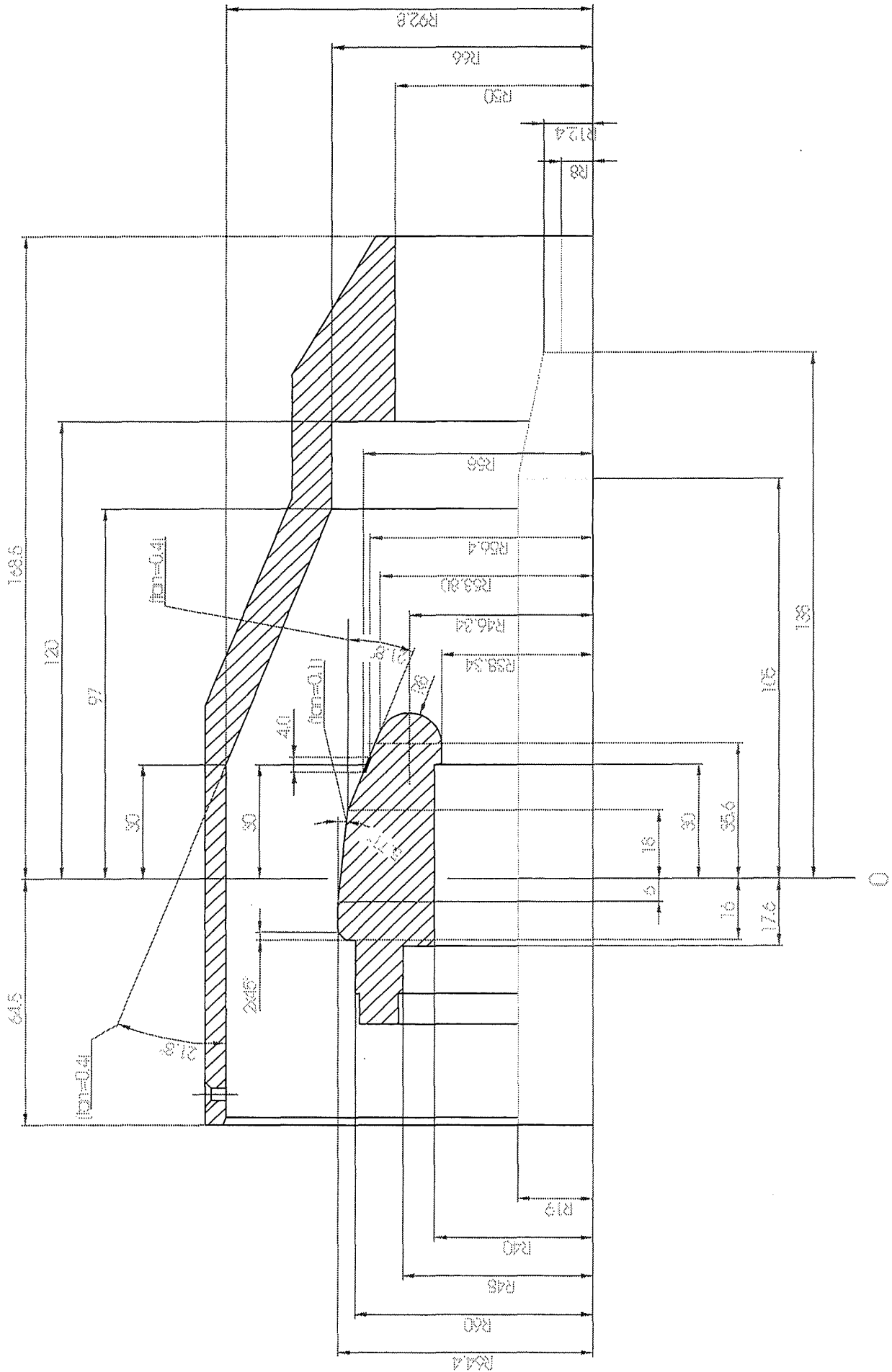
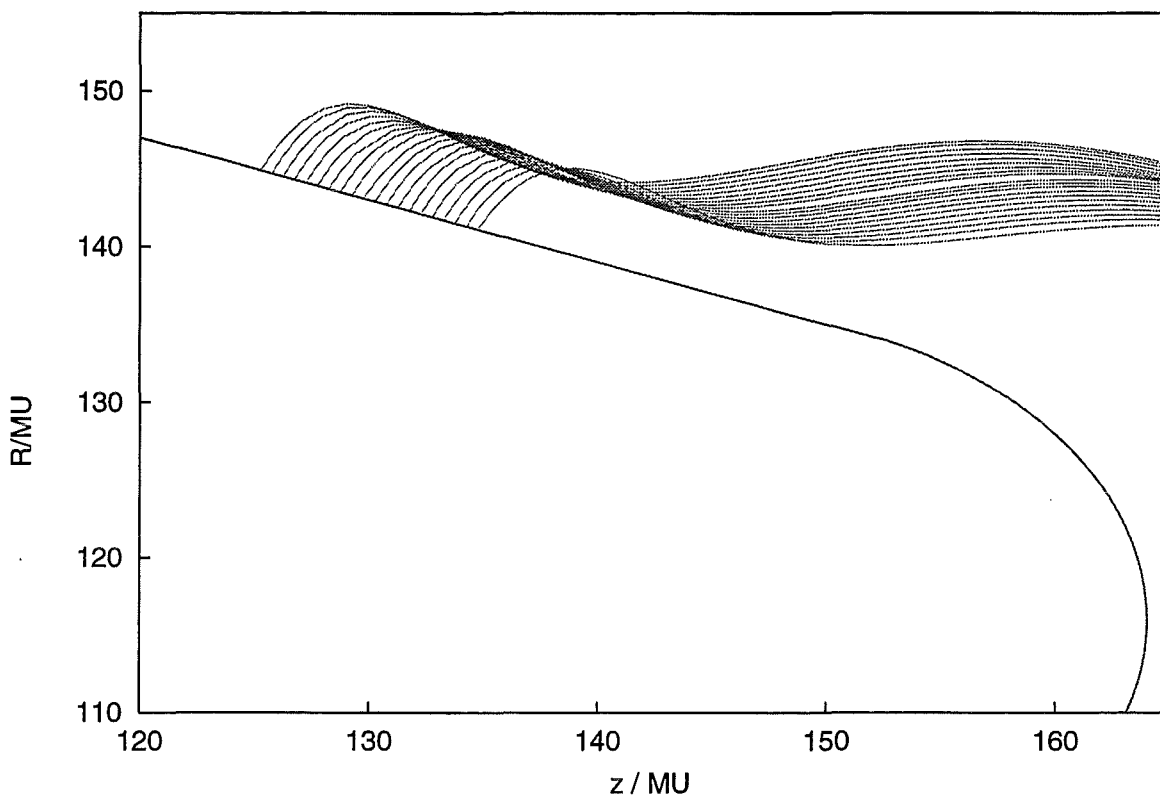
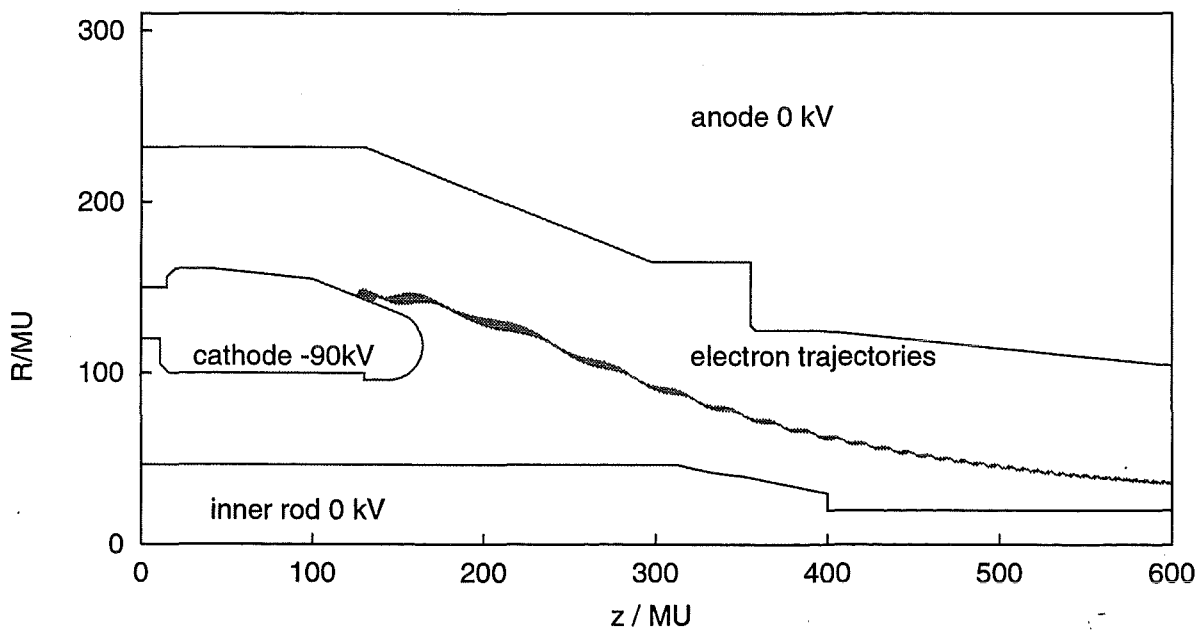


Fig. 1b: Electron gun for the $TE_{31,17}$ mode - layout of the inner contours of the electrodes

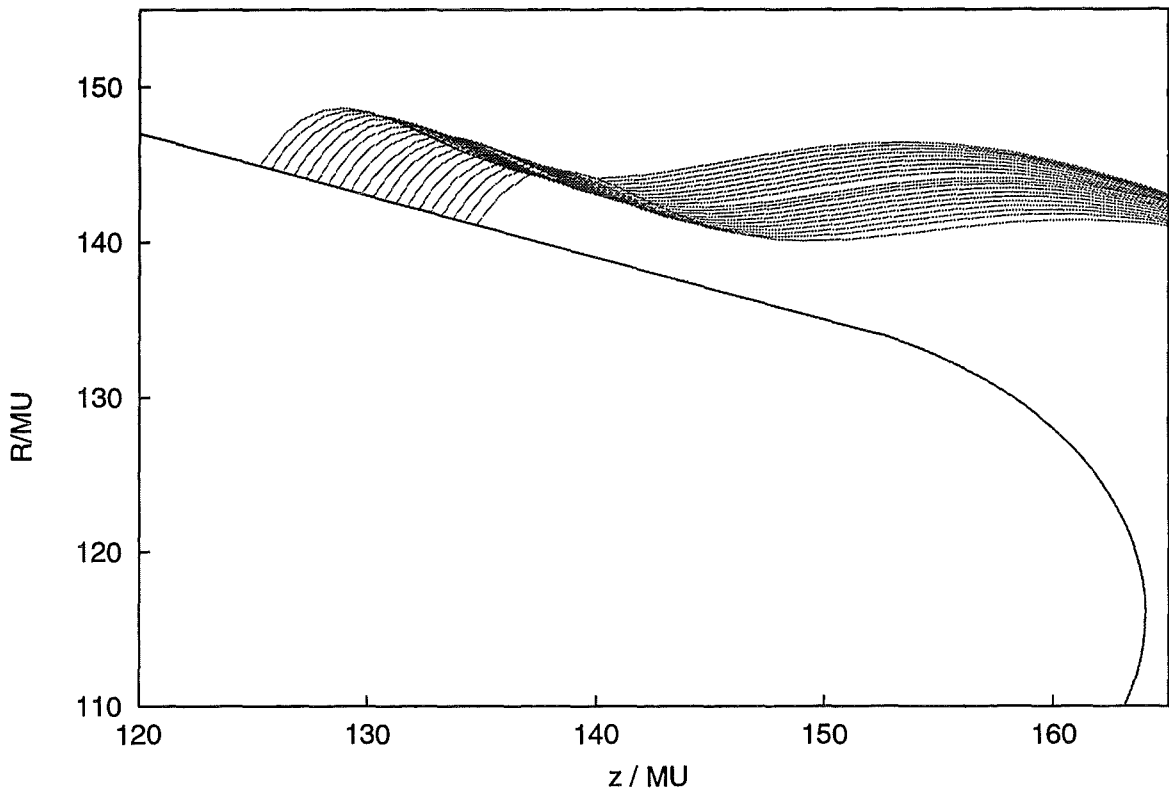


(b) trajectories near the emitter -enlarged scale

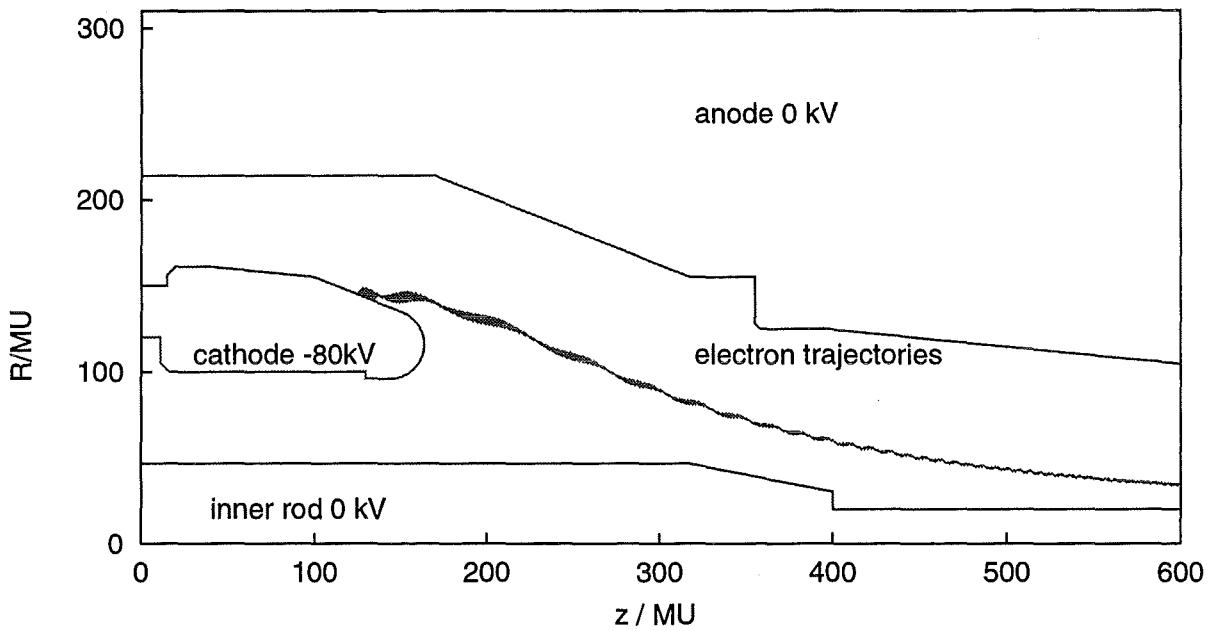


(a) trajectories in the gun

Fig. 3: Electron trajectories at nominal conditions. $1MU = 0.4 \text{ mm}$, $TE_{28,16}$ mode gun.

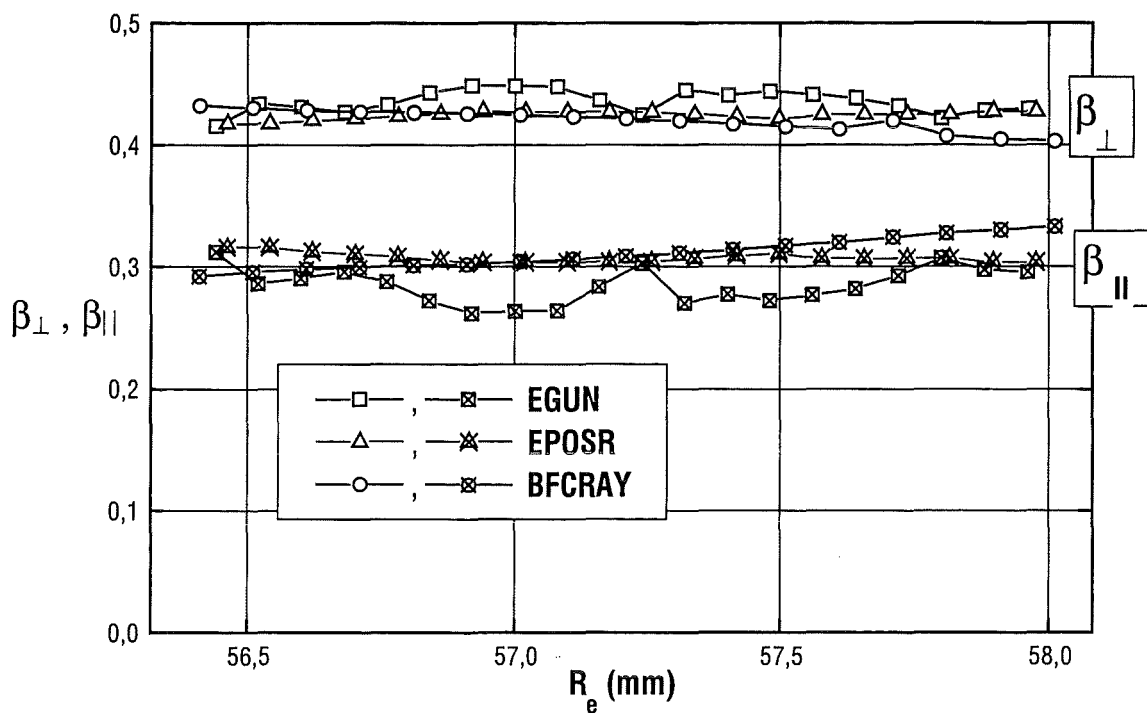


(b) trajectories near the emitter - enlarged scale

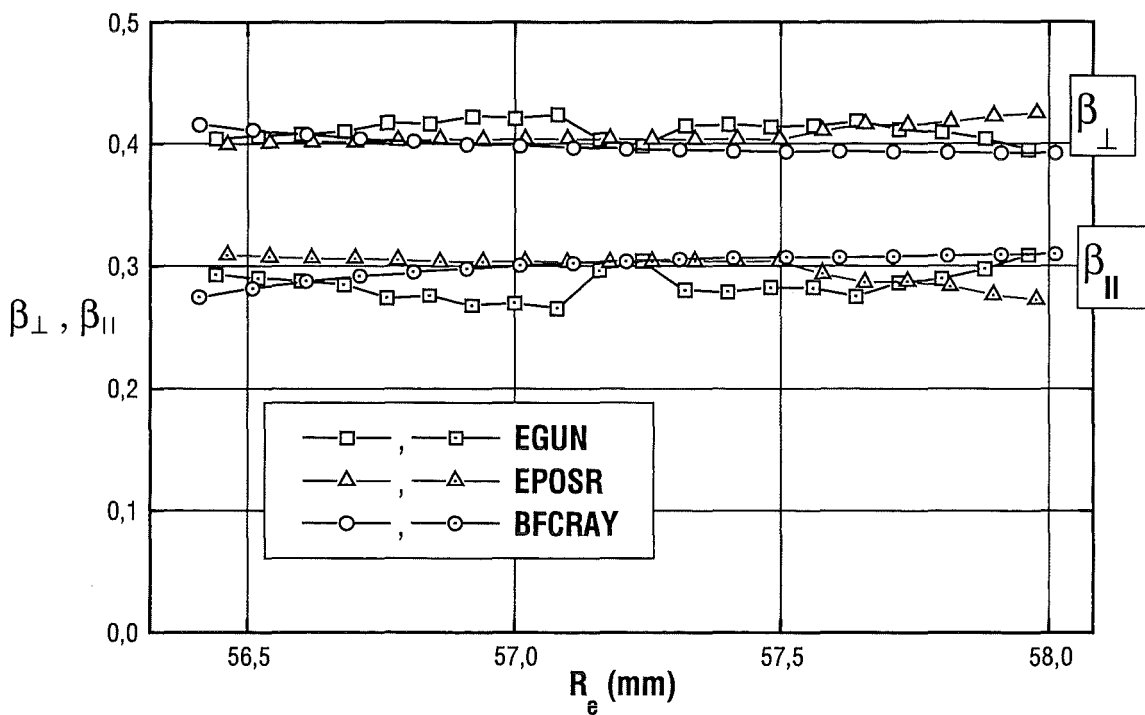


(a) trajectories in the gun

Fig. 4: Electron trajectories at nominal conditions. $1 \text{ MU} = 0.4 \text{ mm}$, $\text{TE}_{31,17}$ mode gun.

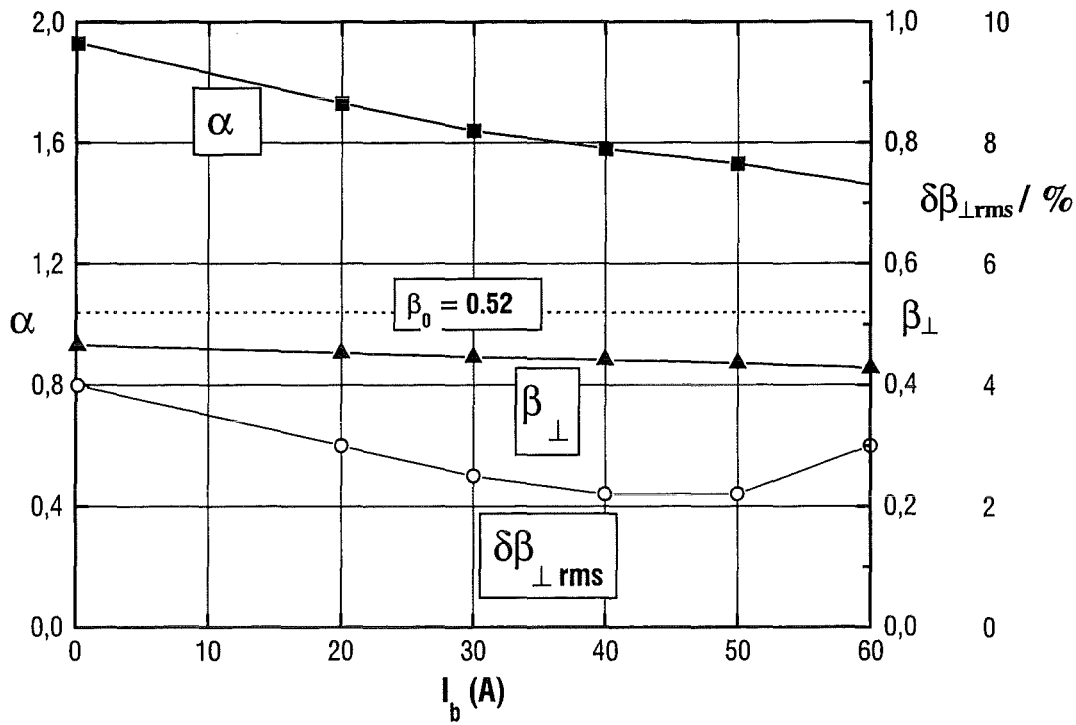


(a) : TE_{28,16} mode gun with $I_b = 50$ A, $U_c = 90$ kV and b2(140)

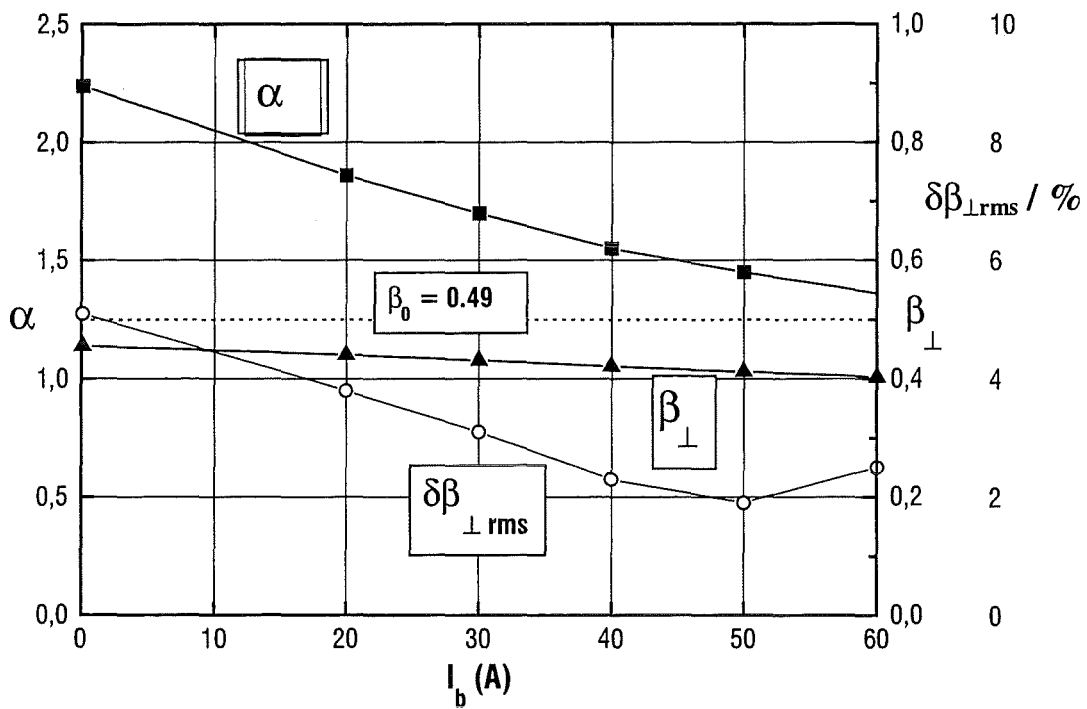


(b) : TE_{31,17} mode gun with $I_b = 50$ A, $U_c = 80$ kV and b2(165)

Fig. 5: The transverse velocity β_{\perp} versus the starting position at the emitter surface calculated for the nominal parameters.

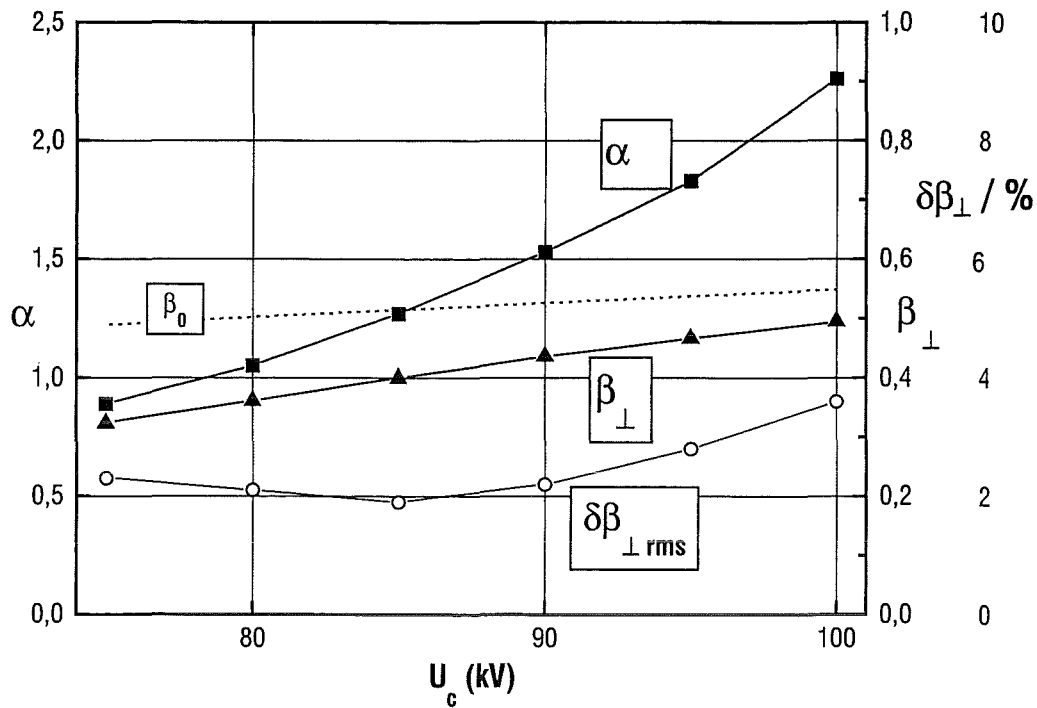


(a) TE_{28,16} mode gun with $U_c = 90$ kV and b2(140)

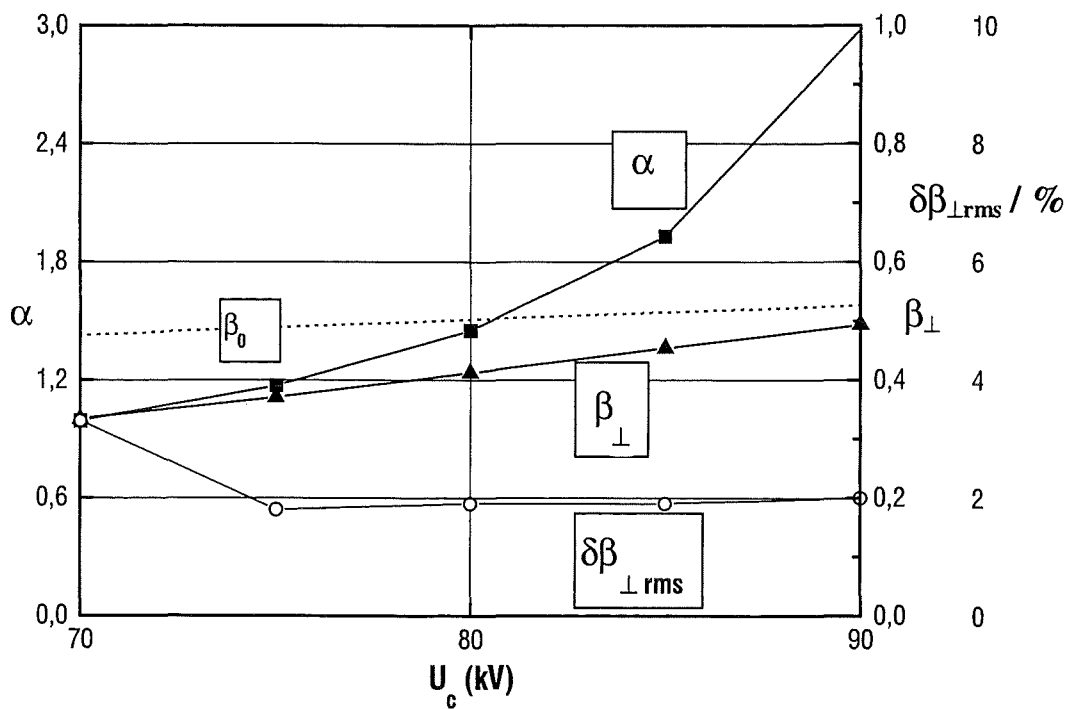


(b) TE_{31,17} mode gun with $U_c = 80$ kV and b2(165)

Fig. 6: α , β_{\perp} and $\delta\beta_{\perp rms}$ versus I_b . β_0 corresponds to the electron energy eU_c .



(a) TE_{28,16} mode gun with $I_b = 50$ A and b2(140)



(b) TE_{31,17} mode gun with $I_b = 50$ A and b2(165)

Fig. 7: α , β_{\perp} and $\delta\beta_{\perp rms}$ versus U_c . β_0 corresponds to the electron energy eU_c .

A 4.5 MW - Electron Gun for a Coaxial Cavity Gyrotron

B. Piosczyk

Forschungszentrum Karlsruhe, Association EURATOM-FZK, Postfach 3640, D-76021 Karlsruhe, Germany,
e-mail: bernhard.piosczyk@itp.fzk.de

Introduction

The mechanical complexity of a coaxial gyrotron is increased due to the existence of the coaxial insert. In order to investigate the related specific problems, in particular in view of cw operation and to demonstrate a technically feasible solution a new electron gun has been designed and is now under fabrication. Since the gun is foreseen to be used in an experimental set up [1] at FZK the design of the gun is adapted to the existing equipment, in particular to the superconducting (sc) magnet.

The electron gun has two electrodes (diode type). The arrangement of the electron emitter ring and the anode is similar to that of a conventional magnetron injection gun (MIG) for gyrotrons. Thus, the emission of the electrons is not, as in the presently used inverse magnetron injection gun (IMIG) directed towards the inner rod [2] but towards the anode. The suggested gun has the following important advantages over the IMIG gun geometry:

- reduced diameter of the gun at a given diameter of the emitter
- negligible influence of the inner rod on the beam properties
- possibility of independent polarization of the inner rod

The design has been performed in order to satisfy the requirements on the electron beam both for the $TE_{28,16}$ mode at 140 GHz and the $TE_{31,17}$ mode at 165 GHz. This can be fulfilled by an individual optimization of the anode shape for both cases with an unchanged surface contours of the cathode and the inner rod.

Requirements on the electron beam and design of the gun

The required parameters are given in the first part of Table 1. The nominal operating voltage has been chosen to be 90 kV and 80 kV, respectively. The needed beam radius R_b in the cavity is different in both cases. Since the cathode radius stays unchanged a different magnetic compression has to be used. The design of the gun has been performed for a magnetic field distribution of an existing sc-magnet consisting of three independently adjustable solenoidal coils, a main coil and two gun coils.

Fig. 1 shows as an example the contours of the electrodes together with the trajectories and potential lines of the gun for the $TE_{28,16}$ mode. The conditions are very similar for the $TE_{31,17}$ mode. Therefore in the following only the case of the $TE_{28,16}$ mode will be considered. β_{\perp} and β_{\parallel} are the normalized transverse and axial

Tab. 1: Nominal electron beam and gun parameters. Results of EPOSR and BFCRAY are in brackets.

operating mode		$TE_{28,16}$	$TE_{31,17}$
frequency :	f / GHz	140	165
beam current	I_b / A	50	50
cathode voltage	U_c / kV	90	80
beam radius at the cavity :	R_b / mm	10.0	9.41
magnetic compression	b	32.7	36.9
magnetic field in the cavity	$B_{\text{cav}} / \text{T}$	5.55	6.58
velocity ratio	$\alpha = \beta_{\perp} / \beta_{\parallel}$	1.53 [1.38/ 1.35]	1.45 [1.38 / 1.33]
velocity spread - rms value	$\delta\beta_{\perp, \text{rms}} / \%$	2.2 [0.7 / 2.0]	1.9 [2.0 / 1.6]

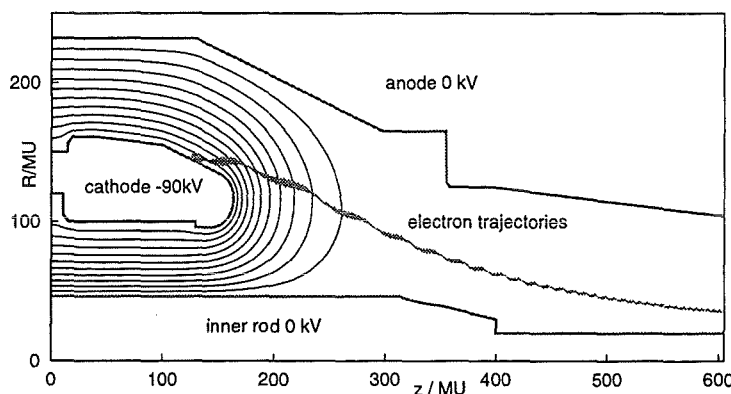


Fig. 1: Electron trajectories at nominal conditions. 1MU = 0.4 mm.

velocities. The average radius of the emitter is 57.2 mm, its tilt angle towards the axis is 21.80° . The coaxial insert is supported from the bottom of the gun. The insert consists of two parts, a rigid outer part which ranges up to the gun region and ends at $z = 400$ MU (Fig.1) and a radially adjustable inner part with a total length of about 120 cm ending approximately 30 cm above the cavity. The range of the radial adjusting is $\Delta r = \pm 2$ mm with a reproducibility of ± 0.1 mm. The adjustment can be performed in the fully assembled tube. The insert has been designed to be sufficiently rigid to keep the amplitude of mechanical vibrations at acceptable values. The part inside and above the cavity is made of copper. The total amount of rf-power dissipated in the insert is about 1 kW at the design rf-output of 1.5 MW. To remove the heat losses water cooling is provided.

Beam and gun parameters under nominal operating conditions

The electron gun has been optimized using the EGUN-code. The trajectories have been calculated from the gun up to the resonator. The electron trajectories are of non-laminar type as shown in Fig. 1.

The nominal beam parameters are given in Tab. 1. The maximum electric field of 6.3 kV/mm is at the nose of the cathode. The electric field at the inner rod is only slightly lower. Compared to that the electric field at the anode is small. At the emitter surface the electric field is about 3.8 kV/mm at zero current and decreases to about 3.5 kV/mm at the nominal current of 50 A. The magnetic compression $b = \{R_c/R_b\}^2$ is defined by the ratio of the radius R_c of the emitter and the beam radius R_b . For the nominal parameters the calculations have been verified with the trajectory codes EPOSR and BFCRAY*. The calculated α -value varies between 5 and 10% for the different codes. Fig. 2 gives the dependence of the transverse and axial velocity versus the starting position at the emitter surface also calculated with the three codes. The agreement of the different calculations is reasonable. In Fig. 3 the dependence of beam parameters on the beam current are given for the $TE_{28,16}$ -mode. The α -value decreases with current and the spread has a minimum around the design current of 50 A.

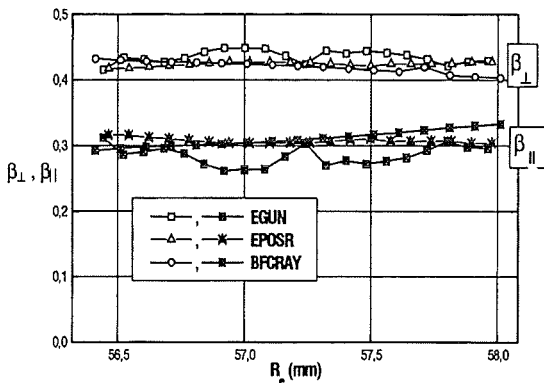


Fig. 2: β_{\perp} and β_{\parallel} versus the starting position at the emitter surface for the $TE_{28,16}$ -mode parameters.

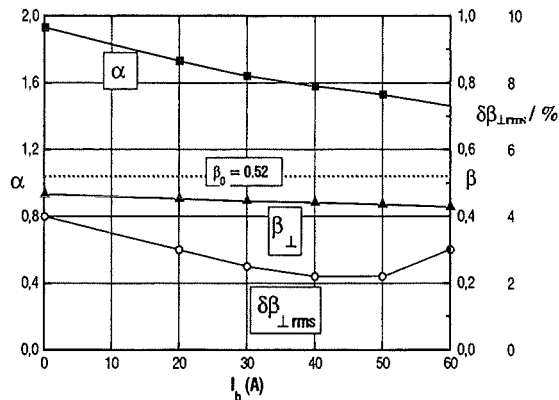


Fig. 3: α , β_{\perp} and $\delta\beta_{\perp,rms}$ versus I_b . β_0 corresponds to the electron energy $eU_c = 90$ keV

Operation of the coaxial gyrotron with a polarized inner rod

In the suggested design the presence of the inner rod enables an operation of the gun with the inner rod polarized with respect to the anode. This allows a variation of the electron beam energy with nearly no influence on the transverse momentum $p_{\perp} \sim \beta_{\perp}$ as has been confirmed in numerical calculations. The operation is similar to that of a three electrode gun (triode gun) where the voltage between the cathode and the modulation anode mainly determines β_{\perp} and the beam energy is given by the voltage between the cathode and the anode. Since according to experimental observations the current I_{rod} to the inner rod is small, $I_{rod} < 0.001 \cdot I_b$, the polarization of the rod can be done nearly powerless. Therefore, an operation with the polarized coaxial insert enhances the efficiency similar as use of a single stage depressed collector without the necessity of having an insulated collector. The polarization of the insert leads to a radial dependence of the potential inside the cavity. This results in an additional energy spread which has been estimated to be below 1% for relevant parameters. However, this has practically no influence on the gyrotron efficiency.

References

[1] B. Piosczyk, et al.: 165 GHz, $TE_{31,17}$ -coaxial cavity gyrotron with quasi-optical rf-output, this conference
 [2] V. Lygin, et al.: Inverse magnetron injection gun for a coaxial cavity 1.5 MW, 140 GHz gyrotron, Int.J.Electronics, 1995, vol.79,2 227-235

* the calculations with EPOSR and BFCRAY have been performed by Dr. V. Manuilov, IAP Nizhny Novgorod and Dr. E. Borie, FZK Karlsruhe, respectively.

165 GHz, TE_{31,17} - Coaxial Cavity Gyrotron with Quasi-Optical RF - Output

B. Piosczyk, O. Braz⁺, G. Dammertz, C.T. Iatrou⁺⁺, M. Kuntze, G. Michel⁺, A. Möbius⁺⁺⁺,
M. Thumm⁺,

Forschungszentrum Karlsruhe, Association EURATOM-FZK, ITP, D-76021 Karlsruhe, Germany
e-mail: bernhard.piosczyk@itp.fzk.de

⁺ also Universität Karlsruhe, Institut für Höchstfrequenztechnik und Elektronik

⁺⁺ National Technical University of Athens, Greece

⁺⁺⁺ IMT GmbH, Luisenstr. 23, D-76344 Eggenstein, Germany

Introduction

A coaxial cavity gyrotron operated at 140 GHz in the TE_{28,16} mode and at 165 GHz in the TE_{31,17} mode with an rf-output power of 1.5 MW is under development at FZK. In order to investigate the basic operating problems in a first step experiments with a gyrotron equipped with an axial waveguide output have been performed. The achieved results were in good agreement with numerical calculations [1,2]. In a second step, the 140 GHz, TE_{28,16} gyrotron has been operated with a dual rf-beam output. For the first time the possibility of internal splitting of the generated rf-power has been demonstrated successfully [3]. The development of rf-windows is progressing very fast. CVD-diamond windows with a transmission capability even above 2 MW at the frequencies considered here seem to be close to realization. Therefore, in the recent experiment the 165 GHz, TE_{31,17} gyrotron has been equipped with a q.o. system for transmission of the rf-power through a single window. The results of this experiment are given here.

Design and experimental set-up

A schematic layout of the gyrotron is shown in Fig.1. With exception of the cavity and the quasi-optical (q.o.) output system the same components are used as in the previous experiments [1-3]. The emitter ring of the electron gun has been renewed since the last experiment because the emission properties of the emitter were

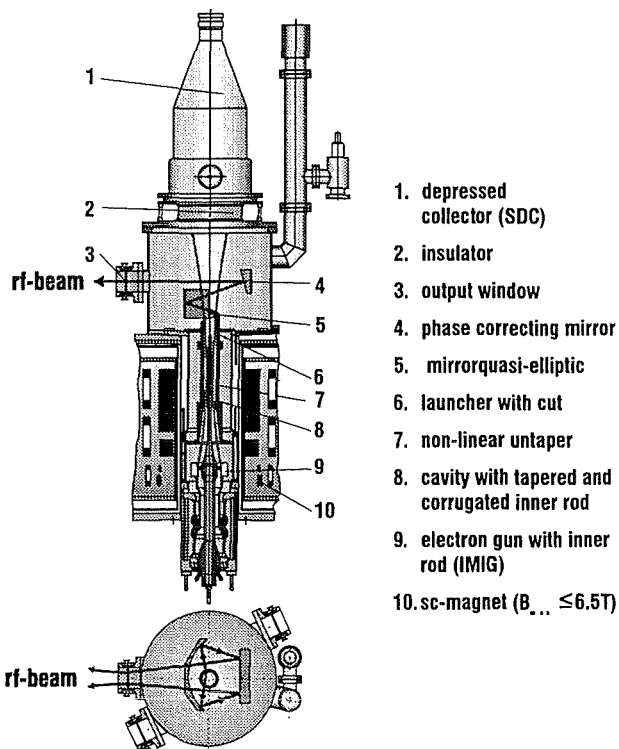


Fig. 1: Schematic layout of the 165 GHz, TE_{31,17} gyrotron

deteriorated due to exposure to air for several times. The dimensions of the TE_{31,17} cavity with the coaxial insert are as in the set-up with the axial rf-output [2]. The high volume cavity mode is directly transformed to a homogeneously distributed paraxial beam. The design of the q.o. system is based on a hybrid geometrical optical and physical optical technique [4]. It consists of a Vlasov launcher with a single cut and two mirrors. The rf-power is radiated with a transverse angle of divergence of about 142° towards the first quasi-elliptic mirror. The second mirror has a phase-correcting surface in order to generate approximately a homogeneous rf-field distribution with a high Gaussian content in the window plane. Since the transmission for neighbouring cavity modes is good, frequency step tuning can be performed. Stray radiation due to diffraction losses has been estimated to ≤ 5% and the absorption losses to about 7% resulting in total losses of about 12%. A fused silica window with a thickness of about 13 half wavelengths at 165 GHz is used. The reflection coefficient was measured to be ≤ 1% at 165 GHz.

Experimental operation and results

The measurements have been performed in pulsed operation. Most data have been taken with an rf-pulse length of 0.5 ms and a repetition rate of 1 Hz. In single pulses the pulse length has been extended up to 15 ms limited by the capability of the HV power supply. The rf-output power P_{out} has been measured calorimetrically. For measuring of the distribution of the rf-output power an infrared camera has been used. The microwave

diagnostic system allows to measure the frequency and to observe whether there is single or multimode oscillation during a pulse. A concentricity of the electron beam relative to the coaxial insert and to the outer cavity wall within ≤ 0.2 mm has been achieved by adjusting as well the sc-magnet and the coaxial insert.

The $TE_{31,17}$ -mode has been found to oscillate with a frequency of 165.0 GHz in very good agreement with the design. A wide single mode operating range has been observed as shown in Fig. 2 for a given magnetic field. The calculated value is in reasonable agreement with the experiment. A maximum rf-output power of 1.2 MW with an efficiency of 25% was measured. The efficiency increased to 35% when operating with the single-stage depressed collector (SDC). Fig.3 gives the rf-output power in dependence of the cathode voltage U_c for a constant magnetic field and an approximately constant beam current. The calculations have been performed with a selfconsistent, time dependent multimode code using the experimental parameters as input. Six neighbouring modes of the $TE_{m,17}$ series have been considered as possible competitors in the calculations. Total rf-losses inside the tube of 12% have been taken into account. At a cathode voltage $U_c \leq 77$ kV the $TE_{32,17}$ mode is oscillating with a frequency $f = 167.24$ GHz. The relatively low value of the measured rf-output power in comparison to the calculations in this mode is presumably due to the rf-reflection of about 14% at the output window. Above $U_c \cong 89$ kV the $TE_{30,17}$ mode oscillating at a frequency of 162.82 GHz is expected. The measured rf-output power in the $TE_{31,17}$ mode is in good agreement with the calculations for $U_c \leq 84$ kV. At cathode voltages above 84 kV the measured rf-power increases slower than the calculated value. The difference between the experiment and calculations rises up to about 15%. Further investigations are needed for clarification.

The rf-power distribution in the window plane is not as homogeneous as expected from the previous design because for the design of the q.o. system partially geometrical optical tools have been used. However, there is good agreement between the measured and the calculated distribution when the calculations are performed fully according to physical optics.

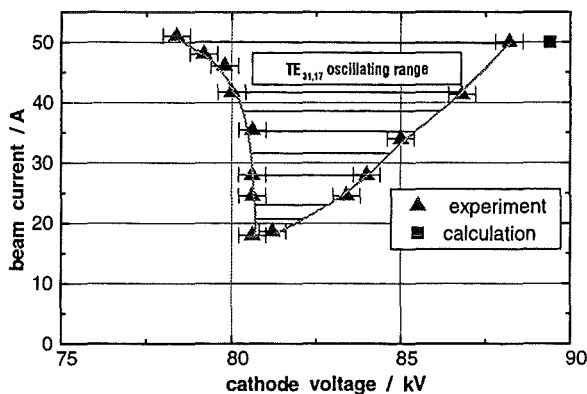


Fig. 2: Single-mode operating range.
 $B_{cav} = 6.55$ T

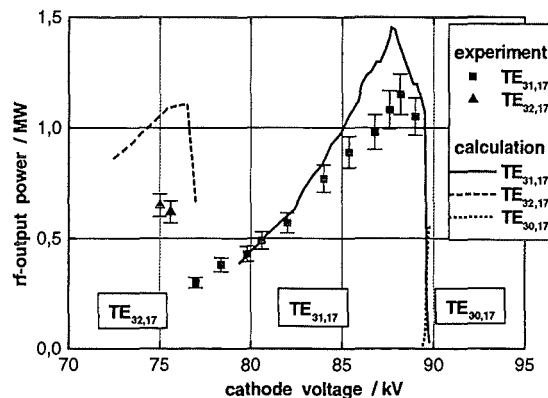


Fig. 3: P_{out} vs. U_c for $I_b \cong 50$ A and $B_{cav} = 6.63$ T
 $\alpha \cong 0.9$ ($U_c = 75$ kV) – 1.1 ($U_c = 87$ kV)

Conclusions and outlook

The measured rf-output power is in good agreement with calculations at lower cathode voltages. At higher values of U_c around the maximum efficiency the experimentally achieved rf-output power is approximately 15% lower than the calculated values. The reason for the observed deviation is not clear yet and needs further investigations. In particular, the influence of rf-power reflection from the output window on the operation will be proved and further calculations of the mode competition will be performed with the multimode code. In order to prove the tools for designing of the q.o. output system the phase correcting mirror has been redesigned fully according to physical optics for a homogeneous field distribution in the window plane and is now under fabrication.

References

- [1] B. Piosczyk et al., "A 1.5-MW, 140-GHz, $TE_{28,16}$ -coaxial cavity gyrotron", *IEEE Transactions on Plasma Science*, **25**(3), 1997, pp. 460-469.
- [2] C.T. Iatrou et al., "Design and experimental operation of a 165 GHz, 1.5 MW coaxial-cavity gyrotron with axial RF output", *IEEE Transactions on Plasma Science*, **25**(3), 1997, pp. 470-479.
- [3] B. Piosczyk et al., "Coaxial cavity gyrotron with dual rf-beam output", *IEEE Transactions on Plasma Science*, **26**(3), 1998.
- [4] G. Michel et al., "Design of a quasi-optical mode converter for a coaxial 165 GHz $TE_{31,17}$ gyrotron", Conf. Digest of the 22nd Int. Conf. Infrared and Millimeter Waves, Wintergreen, Virginia, USA, 1997, pp.25-26.

Design of a Quasi-Optical Mode Converter for a Coaxial 165 GHz $TE_{31,17}$ Gyrotron

G. Michel*, M. Thumm*, D. Wagner†

*) Forschungszentrum Karlsruhe, ITP, Association EURATOM-FZK,
P.O.Box 3640, 76021 Karlsruhe, Germany
and Universität Karlsruhe, IHE, Kaiserstr. 12,
76128 Karlsruhe, Germany

†) Universität Stuttgart, Institut für Plasmaforschung,
Pfaffenwaldring 31, 70569 Stuttgart, Germany

Abstract

The design of a quasi optical mode converter for the extreme volume mode $TE_{31,17}$ is described. It is the operating mode of a 1.5 MW, 165 GHz coaxial cavity gyrotron to be built. The goal is to launch the operating mode directly in order to keep the converter short and the conversion losses and ohmic losses low. Due to the large azimuthal angle of this mode, the design is based on a hybrid geometrical optical and physical optical technique.

Choice of the Converter Principle

The common principle for launching a gaussian like beam from a waveguide cut is the dimple wall converter. It provokes a resonant [1] eigenmode change in the waveguide before launching the beam. For the $TE_{31,17}$ mode this can be easily achieved for a pentagram like ray structure ($\Delta m = 5$) which is well suited for a double beam launcher.

For a single beam launcher, the large spread angle ($2\theta = 140^\circ$) cannot be transformed into a small one with a short converter and the mode $TE_{31,17}$ as the main mode. Since a dimple wall launcher has only little advantage in this case, an ordinary Vlasov launcher is used and the transformation of the strongly divergent beam into a paraxial one is done by means of specific mirrors. This transformation requires either a few weakly curved mirrors [2] or one strongly curved mirror.

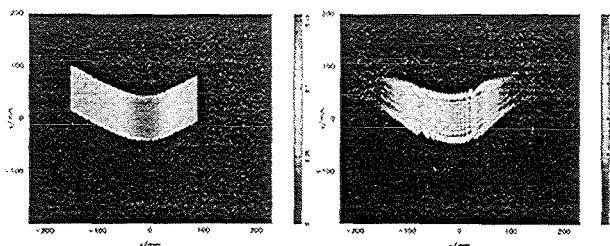


Figure 1: GO (left) and PO (right) Output of the Vlasov Launcher

In the gyrotron vacuum vessel space is limited, therefore the second solution is chosen. The strongly curved mirror, however, cannot be considered as a phase corrector in the sense of a thin lens and must be designed by means of geometrical optics. Here the Vlasov converter has the advantage that it can be easily analysed with geometrical optics. Figure 1 shows the output of the Vlasov converter calculated with the Bessel function and

physical optics and with geometrical optics in the input plane of the quasi parabolic mirror.

The good agreement (except from the fine structure) comes from the high Fresnel number ($N \approx 140$). Because of the strong curvature and the large longitudinal extent of the mirror, it should not be considered as a phase corrector and it corresponds rather to a thick lens.

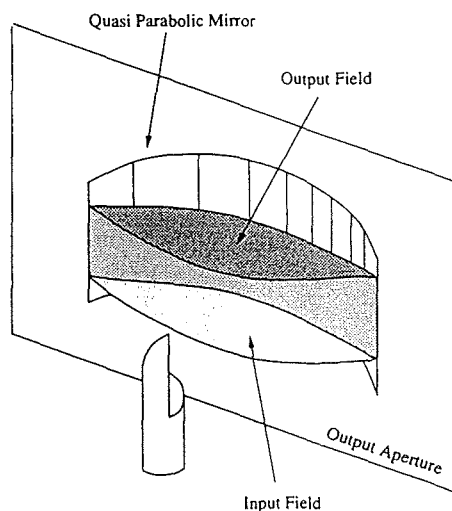


Figure 2: Output Aperture of the Quasi Parabolic Mirror

Therefore the output of the mirror is calculated with geometrical optics in the same aperture as the input (Figure 2). From here, we have a paraxial beam and can continue with physical optics. Figure 3 shows the final setup. A second ("turning") mirror directs the beam out of the gyrotron window.

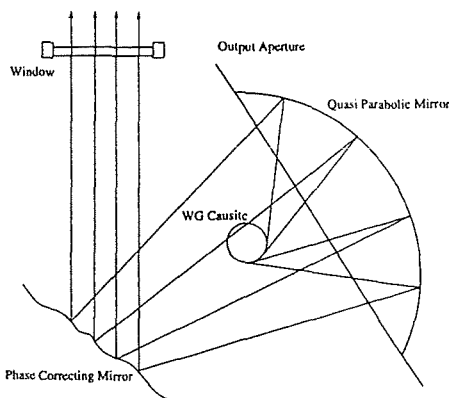


Figure 3: Setup of the Quasi Optical Mode Converter

Design of the Second Mirror

The turning mirror is designed by means of the well known error reduction algorithm [3]. For technical reasons, the gyrotron window is off axis. Therefore it must be turned around two axes. Since the beam has a large transverse extent and a large tilt angle, it is desirable to use the field in the mirror plane for the synthesis instead of the perpendicular lens approximation. This is achieved with a new propagation formula which allows the source as well as the target aperture to be rotated around all three axes. For the forward transform we get in spectral domain

$$\begin{aligned} \hat{U}(\hat{f}^1, \hat{f}^2, d) = \\ \frac{-1}{\hat{f}^3} \hat{U}(\bar{a}_k^1 b_j^k \hat{f}^j, \bar{a}_k^2 b_j^k \hat{f}^j, 0) \beta(-\bar{a}_k^3 b_j^k \hat{f}^j) e^{j2\pi d \bar{b}_j^3 \hat{f}^j} \end{aligned} \quad (1)$$

and for the backward transform

$$\begin{aligned} \bar{U}(\hat{f}^1, \hat{f}^2, 0) = \\ \frac{-1}{\hat{f}^3} \bar{U}(\bar{b}_k^1 a_j^k \hat{f}^j, \bar{b}_k^2 a_j^k \hat{f}^j, d) \beta(-\bar{b}_k^3 a_j^k \hat{f}^j) e^{-j2\pi d \bar{a}_j^3 \hat{f}^j}. \end{aligned} \quad (2)$$

Here, \bar{a} and \bar{b} are the turning dyads of the source and the target aperture, β is the ramp function, d is the distance between the apertures and $\hat{f}^3 = -\sqrt{\lambda^{-2} - (\hat{f}^1)^2 - (\hat{f}^2)^2}$. A detailed derivation of the formulae is given in [4].

In addition, (1) allows to define the target distribution on a tilted mirror. Applications in general antenna engineering or optics suggest themselves.

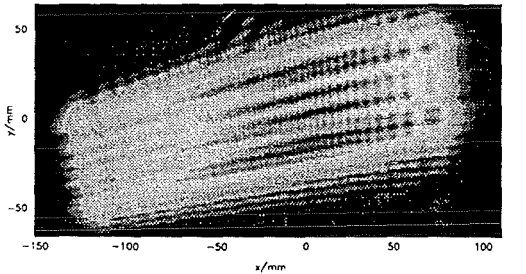


Figure 3: Input Field on the 2nd Mirror

The design goal for the second mirror is a homogeneous field distribution on the window on the one hand and a high gaussian content at some distance after the window on the other hand. Since the input field (see Figure 3) is already relatively homogeneous, both goals can be achieved with this mirror (Figure 4). At the position with the highest gaussian amplitude content, another phase correcting mirror will be placed.

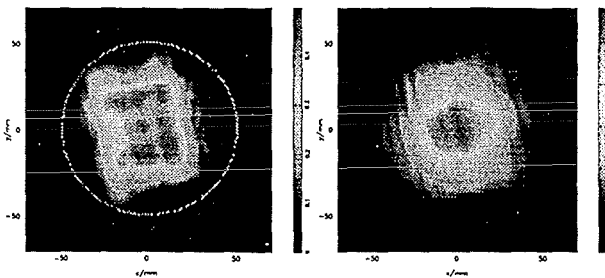


Figure 4: Field Distribution on the Window (left) and 40cm behind the Window (right)

Because of mechanical tolerances and the geometrical optical approximation on the first mirror, the real field distribution will not be as gaussian as in Figure 4. Therefore after the manufacture of the gyrotron the beam will be reconstructed by means of the error reduction algorithm [3] using (1) for oblique view angle correction. Then a pair of two phase correcting mirrors will be placed at the position with the highest gaussian content in order to match the beam to a standard transmission line with elliptical mirrors or a corrugated waveguide.

The actual problem in the design of phase correcting mirrors is the unwrapping of the phase corrector in order to get a smooth mirror surface. However, in most cases this is an ill-posed problem and an exact unwrapping without phase jumps is not possible.

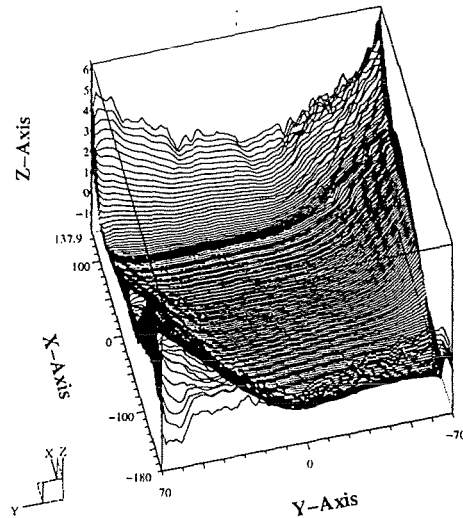


Figure 5: Contour of the Second Mirror

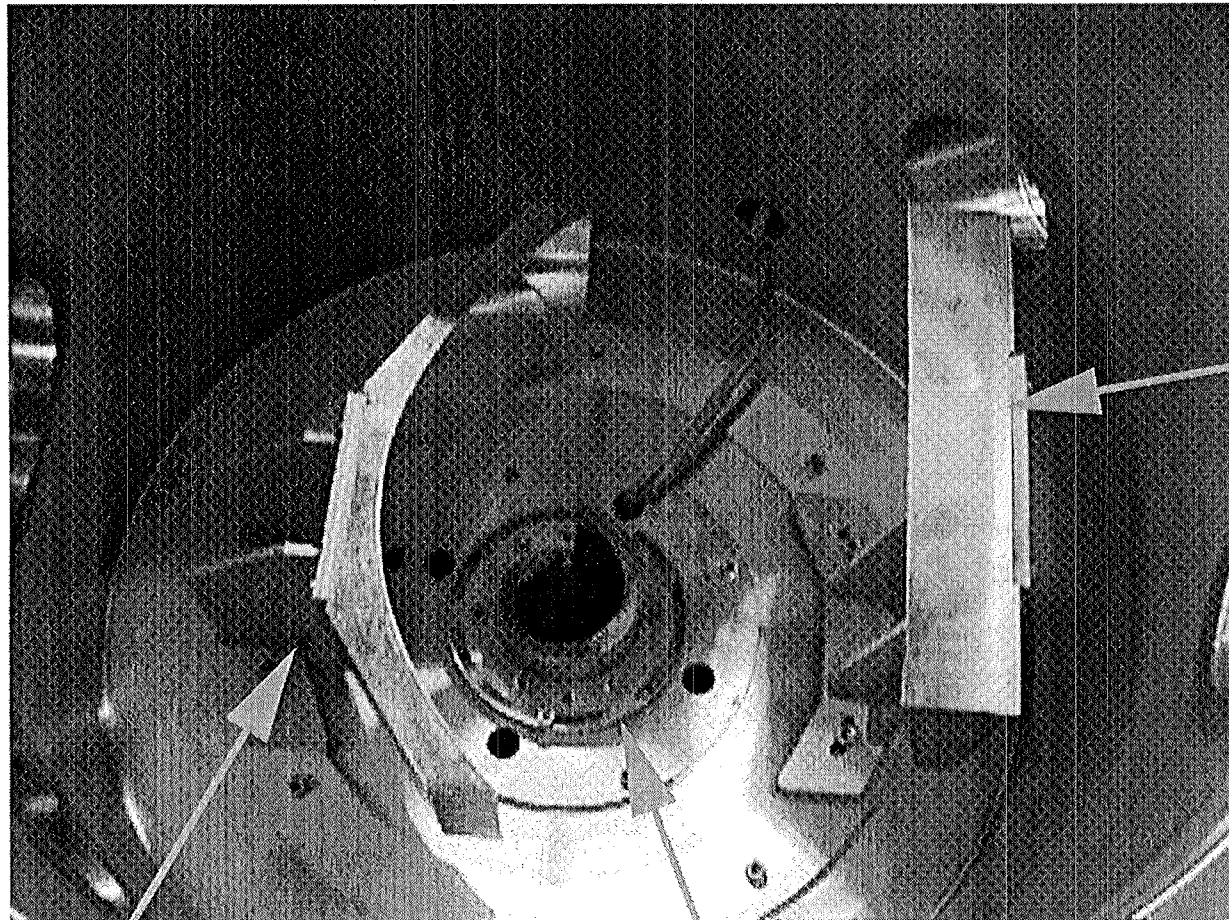
To overcome this problem, a new pathless algorithm was developed which always produces a smooth surface (Figure 5). For ill-posed problems it yields a least squares solution (as a side effect, this is good for compensating noise) and for well-posed problems it yields the exact unwrapped phase corrector. Hence, the algorithm is also interesting for interferometry. A detailed description is published in [4].

References

- [1] G. G. Denisov, S. V. Kuzikov, *Eigenmodes Evolution Due to Changing the Shape of the Waveguide Cross-Section*, Int. J. of IR and MM-Waves, Vol. 18 (1997), No. 3
- [2] Y. Hirata et. al., *Wave Beam Shaping Using Multiple Phase-Correction Mirrors*, IEEE Trans. on Microwave Theory and Techniques, Vol. 45 (1997), No. 1
- [3] B. Z. Katzenelenbaum, V. V. Semenov, *Synthesis of the Phase Correctors forming a given Field*, Radiotekhnika i Elektronika 12/1967, p.244
- [4] G. Michel, E. Sanchez, *Investigations on Transmission Lines with Nonquadratic Mirrors*, 10th Joint Workshop on ECE and ECRH, 6-11 April 1997, Ameland, The Netherlands

Photograph of the Ouasi-Optical Converter

Photograph of the quasi-optical $TE_{31,17}$ -to-wave beam converter



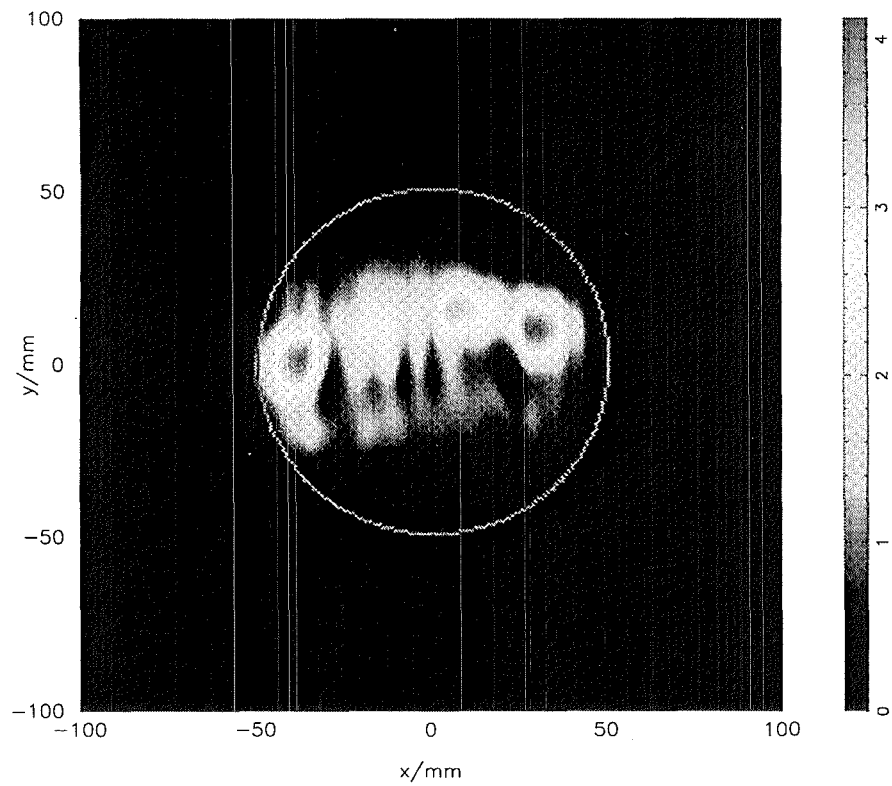
Output Window

Phase Corr.
Mirror

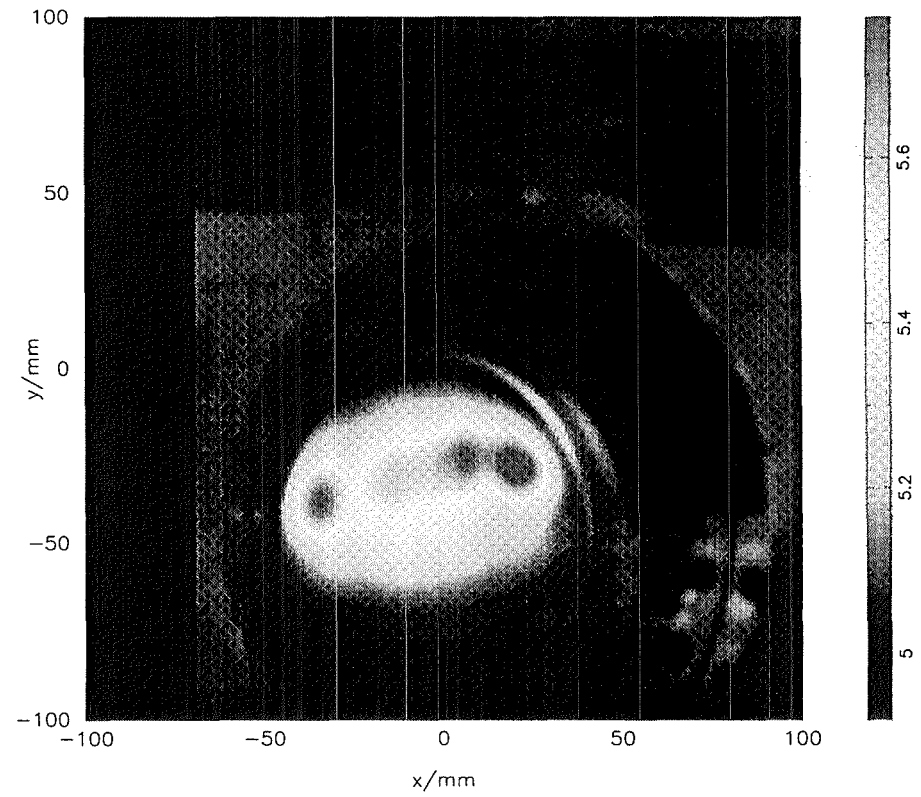
Quasi-Elliptical Mirror

Vlasov Antenna

Calculated Power Distribution
in the Window



Thermal View of the Window



Comparison of measured and calculated rf-power distribution in the window
plane